UNIVERSITY OF LEEDS

This is a repository copy of *Variations in carbonate-evaporite shoreline and ramp facies trends: Middle Miocene Fatha Formation, Kurdistan Region, NE Iraq*.

White Rose Research Online URL for this paper:
https://eprints.whiterose.ac.uk/177325/

Version: Accepted Version

Article:
Abdullah, H, Collier, R orcid.org/0000-0002-8001-0510 and Mountney, N (2021) Variations in carbonate-evaporite shoreline and ramp facies trends: Middle Miocene Fatha Formation, Kurdistan Region, NE Iraq. Journal of African Earth Sciences, 184. 104351. ISSN 1464-343X

https://doi.org/10.1016/j.jafrearsci.2021.104351

© 2021, Elsevier. This manuscript version is made available under the CC-BY-NC-ND 4.0 license http://creativecommons.org/licenses/by-nc-nd/4.0/.

Reuse
This article is distributed under the terms of the Creative Commons Attribution-NonCommercial-NoDerivs (CC BY-NC-ND) licence. This licence only allows you to download this work and share it with others as long as you credit the authors, but you can't change the article in any way or use it commercially. More information and the full terms of the licence here: https://creativecommons.org/licenses/

Takedown
If you consider content in White Rose Research Online to be in breach of UK law, please notify us by emailing eprints@whiterose.ac.uk including the URL of the record and the reason for the withdrawal request.

White Rose university consortium
Universities of Leeds, Sheffield & York

eprints@whiterose.ac.uk
https://eprints.whiterose.ac.uk/

Variations in carbonate-evaporite shoreline and ramp facies trends: Middle Miocene Fatha Formation, Kurdistan Region, NE Iraq

Heero Abdullah [1,2]*, Richard Collier [1], Nigel Mountney [1]

[1] School of Earth and Environment, University of Leeds, Leeds, LS2 9JT, United Kingdom

[2] Now at: Department of General Sciences, College of Education and Languages, Charmo University, Peshawa Street, Chamchamal/Sulaimani, Kurdistan Region, NE Iraq

*heero.abdullah@charmouniversity.org

Abstract

A sedimentological investigation of Miocene deposits at the periphery of the Zagros foreland basin, Kurdistan Region, NE Iraq, reveals a cyclical arrangement of carbonate-evaporite ramp facies. The study aims to provide rare insight into the lateral variability of microfacies and environments of such systems' inner ramp and shoreline. Between 10 and 40 depositional cycles are preserved, separated by a flooding surface, and recording an overall basinward progradation. In each cycle, a shallowing-upward trend from a lower-energy calcareous mudstone and mudstone-wackestone carbonate microfacies at the base to a higher-energy packstone-grainstone-rudstone or low-energy algal mat/stromatolitic carbonate microfacies above is evident. Evaporite deposits of supratidal sabkha origin cap each carbonate deposit. Red clastic sediments that advanced south-westward into the basin from the adjacent Zagros hinterland overlie each evaporite deposit. A flooding surface and return to calcareous mudstones mark the start of the next cycle. Outcrop and thin-section analysis of the carbonate deposits of each cycle reveals a shoaling-up to inner-ramp facies with varied environmental settings that developed under a range of hydrodynamic conditions. Microfacies analysis indicates that these environments included normal marine salinity open lagoons, hypersaline lagoons, restricted and shallow lagoons, sand shoals, intertidal and supratidal flats, supratidal ponds, and a coastal alluvial plain that included channelised deposits and palaeosols. The cyclical facies trend changes toward the top of the succession in that the relative rate of siliciclastic supply markedly increased, whereas the rate of carbonate and evaporite production decreased. Progradation and shoreline migration through time caused lateral and

vertical facies changes and thickness variations over the succession. Repeated relative sea-level changes, associated changes in climate, and variations in sediment supply from the hinterlands during the collision of the Arabian and Iranian plates, combined with a variable rate of accommodation generation, are inferred to have controlled the preserved cyclicity.

Keywords: carbonate ramp, carbonate-evaporite cycles, Miocene, Fatha Formation

1. Introduction

The Miocene Fatha Formation in the Kurdistan Region and related time-equivalent successions in Iran record an example of an ancient mixed carbonate-evaporite ramp that covered much of the northeast margin of the Arabian Plate. This succession forms an important hydrocarbon reservoir and seal system in Syria, Iraq, and Iran (Aqrawi, 1993; Goff et al., 1995). The succession consists of many carbonate-evaporite cycles, variable in nature and thickness from the margin to the depocentre of the basin. At the margin of the basin, the cycles are composed of calcareous mudstone (marl), carbonate, evaporite, and red clastic mudstone units. By contrast, towards the depocentre of the basin, the lateral equivalents of the cycles are composed of marl, carbonate, and evaporites, with the only occurrence of red clastic mudstone being as minor accumulations in the upper part of cycles in the upper member of the formation (Aqrawi et al., 2010).

With its characteristic carbonate-evaporite cycles, the depositional environment of the formation has been the subject of debate. Some researchers concluded that marl, limestone, and evaporite units were deposited in subtidal, intertidal, and sabkha supratidal settings, respectively (Shawkat and Tucker, 1978; Shawkat, 1979; Aqrawi, 1993; Tucker, 1999). However, other researchers have argued that the formation was deposited in a relatively rapidly subsiding basin, separated from an adjacent open seaway by tectonic barriers (van Bellen et al., 1959; Buday, 1980). Furthermore, Ajel (2004) argued that sedimentary features indicative of sabkha environments, such as stromatolites and dolomites, are not abundant in the formation and concluded that sabkha sub-environments were not widespread across the region. Instead, an interpretation of a marine-connected, restricted lagoonal environment was favoured. Hamid (1994) proposed a model for a semi-restricted lagoonal setting. A further study argued that the formation accumulated in a storm-affected evaporitic basin subjected to freshwater influxes (Ameen and Karim, 2007). Moreover,

other studies have documented a stratigraphic equivalent to the Fatha Formation, the Gachsaran Formation in Iran, which is also characterized by shallowing-upward cycles capped by evaporites that are interpreted to have accumulated in supratidal and sabkha environments (James and Wynd, 1965; Gill and Ala, 1972; Pirouz et al., 2011; Soleimani, 2015; Marandi, 2019; Mahmoodabadi, 2020). Thus, the origin and environmental significance of the preserved cycles of the Fatha Formation remain contentious.

This study aims to determine the depositional environments of the mixed carbonate-evaporite cycles of the Fatha Formation and to present a model with which to account for the lateral variation in the expected facies trends when compared to generalised 2D models of ramp systems (Wright, 1986; Burchette and Wright, 1992; Alsharhan and Kendall, 2003; Flugel, 2004). For this purpose, nine stratigraphic outcrops were logged in the Kurdistan Region, Sulaimani city (Fig. 1). This study presents the evaluation and correlation of carbonate-evaporite cycles of regional extent, which can be correlated into the adjacent countries of Iran and Syria, and therefore assists in constraining the broader palaeogeography concerning plate tectonic configuration across the wider region.

2. Geological setting

The Fatha Formation (previously termed the Lower Fars Formation) was initially defined and described by Busk and Mayo (1918) and later reviewed by van Bellen et al. (1959), in Iran, as part of the Fars Group. The Fars Group from Iran was divided into the Lower, Middle, and Upper Fars formations. Lithologically, the Lower Fars Formation (Fatha Formation) was also recognized in Iraq and was named after its Iranian equivalent (van Bellen et al., 1959). Then, a new type section was described in Iraq on the south-western flank of Makhul Mountain, in Al-Fatha Gorge. This was used as the basis for the definition of the Fatha Formation by Al-Rawi et al. (1993).

The Fatha (Gachsaran, Iran) Formation is widely exposed along the northeastern margin of the Zagros foreland basin (Fig. 1A) and represents a mixed carbonate-evaporite deposit. Stratigraphically, the formation conformably overlies the carbonate-evaporite deposits of the Lower Miocene Jeribe Formation (Fig. 2, 3) (Sissakian et al., 2016; Abdullah et al., 2019). However, in some localities where the Jeribe Formation is absent, it unconformably overlies the Euphrates Formation. The upper contact of the Fatha Formation is gradational and diachronous with the overlying fluvial-sequence of the Injana

Formation (Buday, 1980; Jassim and Goff, 2006). In addition, the Fatha Formation is diachronous at a regional scale, being older toward the SE of the basin (SW Iran) but younger towards the NW of the basin (Iraq to Syria) (Shawkat, 1979).

Tectonically, Iraq is divided into three parallel zones from NE to SW: the Thrust Zone, the Unstable Shelf Zone, and the Stable Shelf Zone. The Unstable Shelf Zone is divided into The Imbricated Zone, The High Folded Zone, and The Low Folded Zone from NE to SW (Buday and Jassim, 1987). The High Folded Zone is characterized by double plunging anticlines and narrow synclines. By contrast, folds of the Low Folded Zone are long and very wide. Geologically, the studied area is located between the High Folded Zone and the Low Folded Zone (Fig 1B). These geological zones are intersected by major transverse faults that influence the types and lateral and vertical variations of the deposits.

The Miocene period spanned deposition of the Euphrates, Jeribe, Fatha, and Injana formations (Iraq) and their regional age-equivalents Gachsaran and Agha Jari formations in Iran, with massive evaporite and salt deposits (Fig. 4). These deposits were accumulated within the Zagros foredeep and foreland that developed due to the strong compression between the Arabia and Eurasia plates (Ziegler, 2001). Due to tectonic movements along the Zagros margin at the end of the Oligocene, the basin system became restricted, resulting in the deposition of the Basal Anhydrite. This is the first indicator of total desiccation of the Miocene basin (Aqrawi et al., 2010). Along the northeastern part of the Zagros foreland basin, siliciclastics and evaporites of the Fatha Formation and its age-equivalent Gachsaran Formation were deposited (Fig. 5). A large amount of conglomerate was incorporated into the Hofuf Formation due to the uplift of the western part of the Arabian shield (Ziegler, 2001). A shallow sea with carbonate deposition covered the Gulf of Aden, and the Red Sea was periodically restricted, which caused the evaporite deposition during the Middle Miocene. The Late Miocene sediments are characterized by transitional, shallow-marine units with sabkha deposits. Subsequently, in the Late Miocene, siliciclastic deposits derived from the Zagros hinterland prograded into the basin. In the Pliocene to Pleistocene, the continent-to-continent collision between the Arabian and Eurasian plates was progressively continued, and most of the Arabian Plate was exposed.

The Fatha Formation is characterized by widespread evaporites (gypsum, anhydrite, and halite) facies, interbedded with carbonate, calcareous mudstone, and red continental clastic units (Buday, 1980). It is a mixed carbonate-evaporite unit that shows a cyclic repetition of lithologies,

comprising red claystone or sandstone, siltstone, mudstone, green marl (calcareous mudstone), gypsum, anhydrite, halite, and thin beds of limestone (Jassim and Goff, 2006). Grabowski and Liu (2009, 2012) determined the age of the formation using strontium stable isotope dating for both carbonate and evaporite units. They determined that the formation accumulated during the Burdigalian, or more specifically, the Middle Burdigalian to Lower Langhian stages (18.5 to 15.6 Ma) (Grabowski and Liu, 2009, 2012). The preserved thickness of the formation changes from the depocentre towards the northeastern part of the basin. Furthermore, the general components and thicknesses of limestones and evaporites change in the same direction (Dunnington, 1958). In Iraq, the formation was deposited in two sub-basins, the Sinjar and Kirkuk sun-basins (Fig. 5B), where the formation reaches its maximum thickness (600 to 900 m), whereas, along most anticlines around Sulaimani city, the formation is 200 to 500 m thick (Jassim and Goff, 2006).

The study area runs very close to the basin margin and is centred on the Sulaimani city in the Kurdistan Region. Three main areas were chosen: the Qishlagh-Sargrma, Garmyan, and Darbandikhan (Fig. 1; Table 1). The first study area is located along the Qishlagh-Sargrma Mountain with an NW-SE trend. The Sargrma Mountain is an asymmetrical double plunging anticline, of which the northeastern limb is steeper than the south-western limb (Ghafur, 2012). This structure extends to the southeast toward the Golan structure and the northwest toward the Bazian structure. As a whole, the Qishlagh-Sargrma structure extends in length to more than 80 km and is 2 to 3 km in width. Three sections have been logged along with this structure: the Takiya, Basara, and Krbchna from NW to SE.

The second study area is around Garmyan, represented by the Azh Dagh and Qara-Wais anticlines. These anticlines are asymmetrical with double plunging folds, with an NW-SE trend and en-echelon fold geometries (Kharajiany, 2008). They are parallel to the Qishlagh-Sargrma Mountain. The Azh Dagh anticline is located at the SE end of the structure, whereas the Qara-Wais anticline is at the NW end. The Azh Dagh section was logged along the Azh Dagh anticline, whereas the Mamlaha and Sangaw sections were logged along the Qara-Wais anticline. In addition, the outlying Kfri section was logged near Kfri town, 57 km SW of the Azh Dagh anticline.

The third study area is located around Darbandikhan town, next to the Darbandikhan Dam, along the NE limb of the Qaradagh anticline. The Darbandikhan section was logged next to the Darbandikhan Dam, whereas the Chnarah section was recorded near Chnarah village.

3. Methods

The nine measured sections sum 1775 m in thickness. They were recorded from the well-exposed Miocene succession in the Kurdistan Region (Fig. 1). The Nine sedimentary sections were measured to characterize lateral and vertical variations between the various rock units (Fig. 2). A total of 615 samples were collected from the studied sections from different lithological units. Of these, 300 thin sections were chosen from the carbonate units and twenty thin sections from calcareous mudstone and evaporite for petrographic analysis. Sixteen carbonate microfacies were described using the Dunham (1962) classification with the modifications of Embry and Klovan (1971). The carbonate microfacies were identified and interpreted to determine specific depositional environments. Microfossils were extracted from 50 samples of the calcareous mudstone unit using the H_2O_2 method (Boltovskoy and Wright, 1976). The microfossils were identified to aid the environmental interpretation. The relative proportions of Rotaliids, Ostracods, and Bryozoans in microfossil assemblages of the carbonate mudstone units from the Mamlaha logged section were evaluated to assess whether there is any vertical change in basinal conditions through the formation. The nature of the preserved cyclicity, including assessment of lateral and vertical variations throughout the succession, and the nature of facies variability within individual cycles, was described for the purpose of developing a depositional model.

4. Sedimentary lithofacies

In this section, the results of microfacies analysis of the four sedimentary lithofacies of the cycles, including calcareous mudstone (marl), carbonate, evaporite, and red clastic unit, are presented in detail. Different fossil associations have been recognized from the calcareous mudstone units. Sixteen carbonate microfacies have been described and summarized (Table 2).

4.1. Calcareous mudstone unit (marl) (CM)

The calcareous mudstone unit comprises 13-24% of the succession, from the most distal to proximal parts of the studied areas. It is characterized by bluish to green colors, fine-grained textures and is generally structureless, though millimetric planar laminations and bioturbation are

locally common. The thickness of this unit within a cycle varies from 0.1 to 4.5 m. The main fossils of the unit include rotaliids (35%), *Ammonia, Neorotalia, Pararotalia, Elphidium* and *Rotalia* (exemplified in Fig. 6A, B), ostracods (30%, Fig. 6C, D), oysters (5%), bivalves (5%), miliolids (5%, Fig. 6E, F), bryozoans (15%, Fig. 6G), and gastropods (5%, Fig. 6H). *Ammonia* and *Rotalia* sizes vary between 200 µm to 600 µm (Fig. 6A, B). The sizes of ostracods change from 250 µm to 1000 µm (Fig. 6C, D), and their morphologies show several kinds of ornamentations, from smooth to moderate/high ornamentations. Miliolids (Fig. 6E, F) and gastropods (Fig. 6H) are also recorded in the samples as a minor component and are associated with the rotaliid group. Planktonic foraminifers are not recorded in the studied sections, though such forms were detected from similar facies in the basin depocentre (Shawkat, 1979).

The calcareous mudstone units from the lower part of the succession include rotaliid group foraminifera, miliolids, and ostracods within a muddy matrix, whereas, toward the upper part of the succession, marine bryozoans and oysters are dominant. Horizontal and vertical *Skolithos* traces are abundant in the marl units in the upper part of the succession. Petrographically, the calcareous mudstone unit includes detrital quartz grains (10%), feldspar (2%), and ferroan dolomite (5%). The percentage of the detrital quartz grains increases toward the top of the individual marl units to approximately 30% (Fig. 7A).

The association of rotaliids with ostracods and miliolids is indicative of a hypersaline lagoonal depositional environment (Abou-Ouf et al., 1988; Gheith and Auf, 1996; Hariri, 2008; Mohamed et al., 2013). Furthermore, rotaliids indicate and have an affinity with saline lagoons and pools (Murray, 1973; Mohamed et al., 2013). The variable size of *Ammonia* likely relates to salinity variations, where with decreasing salinity, the size of *Ammonia* increases (Bradshaw, 1961). The sizes and morphologies of the ostracods from the calcareous mudstone units are variable. Bryozoans live in normal marine water with a salinity of approximately 3.5%, and any salinity fluctuations causing bryozoans to decline (Boersma, 1978; Haq and Boersma, 1998).

Overall, the calcareous mudstone units are interpreted to have been deposited in low-energy muddy hypersaline lagoonal conditions to low-energy, normal marine conditions from the lower to upper parts of the Fatha Formation, respectively. This is evidenced by abundant rotaliids, ostracods, and miliolids, the absence of high-energy sedimentary structures, a muddy matrix,

planar laminations, and bioturbation in the lower and the increase of normal marine bryozoans, oysters, and bioturbation in each unit in the upper part.

4.2. Carbonate lithofacies

The carbonate units are the main component of the Fatha cycles. They range from 0.10 to 5.0 m thick and comprise 5 to 15.5% of the total succession, from the most distal to proximal parts of the studied area.

Table 2 describes the microfacies distinguished in this study based on the sedimentary structures, compositions, skeletal and non-skeletal components. Sixteen carbonate microfacies are distinguished, which themselves can be assigned into five facies associations: low-energy restricted hypersaline lagoon, low-energy very shallow lagoon, shallow lagoon with connection with open-marine, intertidal, near-shore, and ooidal sand shoals (see Table 2 for details).

4.2.1. Low-energy restricted hypersaline lagoon facies association

This facies association is characterized by the presence of restricted high-salinity benthonic foraminifera, including rotaliids and miliolids, muddy matrix, and evaporite pseudomorphs. It includes three main microfacies:

- **Skeletal mudstone and wackestone microfacies (M1-M3)**

This group of microfacies makes up the lower part of each of the carbonate units and constitutes about 10% of the total carbonate microfacies of the succession. It comprises three different microfacies, mudstone (M1), rotaliids wackestone (M2), and miliolids wackestone (M3) (Table 2).

Rotaliids and miliolids, scattered within a muddy matrix, are the main constituents of these three microfacies (Fig. 7B-7D). The sizes of the rotaliids (Fig. 7C) and miliolids (Fig. 7D) reach 300 to 600 µm and 100 to 300 µm, respectively. The matrices of the skeletal mudstone and wackestone microfacies comprise micritic muds which are locally bioturbated. In addition, large evaporite nodules are common, though many have been dissolved to leave vugs 1 to 2 mm in diameter.

The presence of rotaliids indicates hypersaline lagoon conditions (Debenay et al., 2001), whereas miliolids are signs of a restricted lagoon and hypersaline conditions (Geel, 2000). Rotaliids typically live in relatively deeper hypersaline lagoon environments (2 to 14 m water depth) than miliolids, which live to average water depths of 2 m (Hariri, 2008). The presence of evaporite pseudomorphs without evidence for subaerial exposure indicates that the evaporite crystals were probably developed subaqueously, perhaps due to strong brine refluxes (Becker and Bechstädt, 2006). The paucity of foraminifera in terms of diversity and abundance, the high percentage of muds, the lack of evidence for subaerial exposure and the associations of the microfacies together (M1-M3) are collectively indicative of accumulation in a low-energy, restricted hypersaline lagoon setting on an inner ramp.

4.2.2. Shallow lagoon to intertidal facies association

The shallow lagoon to intertidal facies association represents laminated carbonate lithofacies and laminated algal and stromatolites facies. This facies association is characterized by intertidal structures, including microbial laminites, bioturbation, stromatolites, and fenestrate pores. It includes seven carbonate microfacies:

- **Strongly micritized bioclastic packstone (M4)**

This microfacies is documented from the Takiya and Basara sections and constitutes 2% of the total stratigraphic thickness of carbonate microfacies. It is characterized by intense bioturbation and micritization (Fig. 7E). Beds, 0.1 to 0.3 m thick, are evident, but any internal sedimentary structure has been destroyed due to intense bioturbation. The matrix comprises bioturbated carbonate muds, and most of the bioclasts are difficult to recognize due to micritization. However, several miliolids and ostracods were recognized (Fig. 7E). Fenestral pores are seeing between the grains. Quartz grains and evaporite pseudomorphs are absent.

The highly micritized bioclasts and benthic foraminifera such as miliolids and ostracods indicate low energy but well-oxygenated conditions (Flugel, 2004). The presence of shallow water foraminifera (miliolids) and ostracods and low-energy mud matrix with fenestral pores indicate a low-energy, very shallow water and, therefore, intertidal environment.

- **Bioclastic gastropod-bivalve packstone (M5)**

This microfacies is recorded at the top of carbonate units and is commonly associated with skeletal mudstone microfacies M1 and rotaliids wackestone microfacies M2. Beds are 0.4 to 0.5 m thick, and the grain components are of coarse sand grade. This M5 microfacies makes up ~5% of the total carbonate microfacies by stratigraphic thickness. Gastropods and bivalves are the main skeletal components (50-60%) (Fig. 7F). The principal associated bioclasts are echinoids and bryozoans, and the minor associated bioclasts are miliolids, rotaliids, and serpulid worm tubes in a micrite matrix. The sizes of the bivalve shells and gastropods reach 500 to 1500 µm and 1.5 to 2 mm, respectively.

The presence of gastropods and the microfaunal assemblage indicates deposition in shallow lagoonal to intertidal settings (Flugel, 2004). The micritic matrix indicates deposition in a low-energy environment. This microfacies was likely deposited in a low-energy and very-shallow lagoon to an intertidal setting.

- **Bioclastic oyster-barnacle floatstone (M6)**

This microfacies made up ~5% of the total carbonate microfacies by stratigraphic thickness. It is characterized by a coarse floatstone texture with abundant barnacles and oysters (~20% of photomicrograph area) which are greater than 2 mm in size (Fig. 8A) and associated with bivalves (5%), benthic foraminifera (2%), serpulid tubeworms (1%), echinoids (2%), gastropods (2%) and ostracods (2%) in a micrite matrix. The oysters and bivalves have large and complete valves. The oysters and bivalves are *in situ* forms and have complete valves, whereas the barnacles are attached to the oysters and bivalves. Micritic intraclasts and quartz and chert grains are also abundant. Micritic envelopes around the barnacle and oyster shells are also abundant, and the bivalve shells are filled by fine-grained peloidal micrite.

The genus *Ostrea* lives in a less than normal marine salinity, typically about 23‰ (Hudson, 1963). Barnacles live in intertidal environments (Flugel, 2004; Ghosh and Sarkar, 2013). Floatstone textures and the associated bioclasts of oysters, barnacles, and bivalves in a muddy matrix, together with bioturbation and common micritic envelopes, indicate low- to moderate-energy conditions. The abundance of the oysters indicates deposition in less than 35 m depth of brackish, nutrient-

rich and poorly oxygenated water (Gertsch et al., 2010). The occurrence of barnacles with the oysters suggests deposition in intertidal to supratidal waters (Schmitt, 1957). The presence of micritic intraclasts, quartz, and chert grains indicate that the depositional environment was relatively close to the shoreline. The association of barnacles and oysters with abundant micritic intraclasts suggests deposition in normal marine to low salinity waters in very shallow lagoonal to intertidal settings.

- **Laminated fecal pellet grainstone microfacies (M7)**

This microfacies comprises ~2% of the total carbonate microfacies by stratigraphic thickness. Fecal pellets are characterized by dark, rounded to elongate shapes and have relatively uniform sizes. The pellets are less than 300 μm in diameter and make 80-90% of the rock (Fig. 7G, H). Bioclasts are very rare in this microfacies, though a small number of miliolids and *Dentritina* are noted. Rarely, large micritic intraclasts up to 4 mm in diameter are seen, with large fecal pelleted grains up to 1.5 mm in size.

The presence of laminated structures in fine to medium sand-sized fecal pelleted grainstones indicates moderate- to high-energy subtidal to intertidal, lagoonal to back-shoal settings. The pellet preservation indicates meager sedimentation rates and early cementation (Tucker and Wright, 1990). Higher salinity coupled with microbial activity can also lead to rapid lithification and thus increasing preservation potential (Scholle and Ulmer-Scholle, 2003).

- **Microbial algal laminites and laminated mudstone (M8)**

This microfacies is recognized based on visible laminations, including very small peloids (10-30 mm in diameter) due to algal activity (Fig. 8B). It is recorded in most of the studied sections at the top of some carbonate units, comprising up to 10% of the total carbonate microfacies. It is characterized by dark grey, fine-grained carbonate rocks with planar laminations and is commonly spatially associated with stromatolites (Fig. 8C-D). Specifically, the microfacies is frequently overlain by stromatolites which are in turn capped by chicken-wire evaporites.

This microfacies is common in arid intertidal to supratidal depositional environments; for example, it occurs in the arid Trucial Coast (Kinsman and Park, 1976). Laminated algal bindstone with

authigenic evaporite minerals, fenestrae structures, and the associations with stromatolites and chicken-wire evaporites indicate upper intertidal settings in an arid climate (Kendall et al., 2002; Flugel, 2004).

- **Stromatolites (M9)**

The stromatolite microfacies are recorded at the top of carbonate units and comprise about 10% of the total carbonate microfacies by stratigraphic thickness. The stromatolite microfacies (M9) is a domal fenestrae algal bindstone and is interbedded with calcareous mudstone microfacies in the Takiya section (Fig. 8E, F). The rocks of this microfacies are dark grey fine carbonate rocks with visible dome structures on centimetre and millimetre-scale laminations. The fenestrae pores become larger toward the top. In addition, the laminations are cut by a irregular surface at the top (Fig. 8E, F). The thickness of the stromatolite is 10 cm.

The occurrence of fenestrae structures, irregular subaerial exposure at the top of M9 stromatolites (Fig. 8E), and associations with algal mats and nodular evaporites at the top of the carbonate units all indicate intertidal environments in an arid climate. The same facies of stromatolites and algal laminites has been observed in the Fatha Formation in the basin depocentre (Shawkat and Tucker, 1978; Shawkat, 1979). Moreover, fenestral mudstones, stromatolites, and microbial laminites are recorded from the Oligocene-Miocene Asmari Formation in Iran (Amirshahkarami et al., 2007; Vaziri-Moghaddam et al., 2010; Amirshahkarami, 2013).

- **Dolo-mudstone microfacies (M10)**

The dolo-mudstone microfacies is characterized by fine dolomite crystals, approximately 10-20 μm in diameter, with high porosities of approximately 25% (Fig. 8G). This microfacies is recorded at the top of the carbonate units from Takiya and Mamlaha sections and is capped by nodular and chicken-wire evaporites. It makes up ~5% of the total carbonate microfacies in terms of stratigraphic thickness.

The association of dolomite with nodular evaporites and chicken-wire structures is widespread in the modern upper intertidal and lower supratidal zone of the arid Trucial Coast (Alsharhan and

Kendall, 2003). Fine-grained dolomite and associated evaporites in the Fatha Formation are thus interpreted to indicate the upper intertidal zone.

4.2.3. Shallow lagoon with connection with open-marine facies association

This facies association is characterized by benthic foraminifera, including miliolids and rotaliids, with open-marineorganisms, such as echinoids. It represents two main microfacies:

- Ec**hinoid wackestone/packstone (M11)**

This microfacies comprises about 3% of the total carbonate microfacies. Echinoid fragments of both spines and plates (10-20%) are the main bioclasts contained within a muddy matrix (Fig. 8H). The echinoids plates are 500 µm to 2 mm in length; echinoid spines are <300 µm in width. The associated bioclasts in wackestone and packstone textures are miliolids (2% of photomicrograph area), ostracods (2%), and rotaliids (5%). Detrital quartz and chert grains (5%) are evident.

The high percentage of echinoid spines and plates indicates normal marine salinity for the depositional environment (Strasser et al., 1995). The presence of an associated benthic foraminiferal assemblage of miliolids and rotaliids and ostracods indicates a shallow lagoon but connected to open-marine conditions on the inner ramp.

- **Bioclastic peloidal grainstone (M12)**

This microfacies is very common in the carbonate units and constitutes ~10% of the total carbonate microfacies. The main component of this microfacies consists of peloids, which are between 100-200 µm in diameter and make up 70-80% of the rock. This microfacies is characterized by the presence of a high diversity fauna which consists of bivalves (10-20%), ostracods (20-30%), or echinoids (20-30%), with rotaliids (5%), miliolids (5%), bryozoans (2%), and variable proportions of oysters, barnacles and radial ooids (Fig. 9A). The grains are characterized by moderate sorting and high-packing order within a sparite cement. The echinoid plates are wholly or partially micritized and are larger than 500 µm in diameter. The ooids are radial, smaller than 250 µm in diameter, and form up to 10% of the rock.

The peloids resulted from partial or total micritization of bioclasts and ooids. The bioclasts indicate normal marine salinity, given high percentages of echinoids (Strasser et al., 1995). Early mechanical compaction, indicated by a relatively high-packing order of grains, indicates an original absence of mud. The moderately sorted grain sizes, small-sized foraminifera, grainstone texture, and high diversity of fauna indicate that the facies was deposited in a shallow lagoon connected to open marine conditions within the fair-weather wave base.

4.2.4. Near-shore facies association

Near-shore facies association is characterized by the presence of wave-agitated structures and sparite matrices. Moreover, the presence of quartz minerals is an indicator of a mixed carbonate-clastic depositional setting. In this facies association can be distinguished three kinds of microfacies:

- **Bivalve rudstone (M13)**

This microfacies comprises ~5% of the total carbonate microfacies. Bivalve shells are the main component of this microfacies (80%-90%). The rudstone microfacies is characterized by very coarse, fossiliferous carbonate, rich in bivalves, which reach up to 15 mm in diameter (Fig. 9B). The associated carbonate components are miliolids, rotaliids, ostracods, gastropods, barnacles, oysters, and red algae in a sparite matrix. Weak planar laminations and ripple marks are seen in this microfacies (Fig. 9C).

The presence of large bivalves in a rudstone texture indicates wave-agitated, near-shore environments (Flugel, 2004). The lack of mud and the presence of ripple marks indicate deposition and winnowing above the fair-weather wave base (Flugel, 2004). The preservation of large and complete bivalves in combination with oysters indicates in situ accumulation of skeletal materials.

- **Peloidal-ooidal grainstone (M14)**

This microfacies makes up ~3% of the total carbonate microfacies. It is characterized by micritized and concentric ooids anddark fecal pellets (Fig. 9D). The fecal pellets form ~50%, and the ooids make ~40% of the microfacies in a sparitic matrix. The fecal pellets are 100-400 µm in diameter

and are dark and rounded, and elongate or rod-shaped. Whereas, the ooids are 200-600 µm in diameter and are moderately sorted. Some of the ooids are concentric normal ooids. However, others are micritized or superficial ooids with incomplete or thin cortical coatings. The nuclei of some ooids are fecal pellets but most of the 'ooids' nuclei are dissolved and form intraparticle porosity.

The bioclastic ooidal and ooidal grainstone microfacies, the presence of pellets, the lack of mud, the presence of ooids, and the poor to moderate sorting indicate moderate-energy conditions in the shoreface zone or at the edges of sand shoals, above the fair-weather wave base on the inner ramp.

- **Sandy carbonate, bioclastic calcarenite microfacies (M15)**

This microfacies is characterized by mixed siliciclastic and carbonate components and comprises ~15% of the total carbonate microfacies of the succession. The grain sizes vary from fine to coarse sand and are associated with different bioclasts such as miliolids, rotaliids (Fig. 9E), ostracods, barnacles, bivalves, echinoids, and oysters. Quartz and chert grains, feldspar minerals, lithoclasts, and bioclasts are the main components of the facies. The thickest unit of this microfacies is recorded from the more proximal locations represented by the Basara and Darbandikhan sections. Toward the more distal southwest area of the basin, this microfacies is not well-preserved. The rocks of this microfacies are characterized by a grey dark-grey to greenish color with planar laminations, graded bedding, and ripple marks (Fig. 9F).

The presence of the sandy calcarenite microfacies with sedimentary structures such as planar laminations indicate deposition above the fair-weather wave base in an area influenced by wave action in a marginal inner ramp setting (Thrana and Talbot, 2006). The predominance of quartz, chert, feldspar minerals, lithoclasts, and different bioclasts indicates mixed carbonate-siliciclastic facies near the shoreline.

4.2.5. Ooidal sand shoal facies association

Ooidal sand shoal facies association is characterized by the occurrence of ooids with a high-energy wave and current sedimentary structures. This facies association represents ooida grainstone microfacies

- **Oolitic grainstone (M16)**

This microfacies comprises ~15% of the total carbonate microfacies by stratigraphic thickness and is recorded in all the studied sections as outlined in Table 2. The ooids (M16) are mostly between 300 and 500 µm in diameter (Fig. 9G, H). They are rounded to ellipsoidal and exhibit moderate to good sorting. In addition, they are mostly normal ooids (on average 90%) with a few micritized, distorted (Carozzi, 1961) and superficial ooids (10%). However, the ooidal microfacies rarely comprise 80-90% of distorted, superficial, and micritized ooids. Foraminifera (Fig. 9G), quartz, chert, pellets, and mollusks make up the nuclei of the ooids dissolved to form secondary porosities (Fig. 10A). However, the nuclei of some ooids are filled with micritic cement (Fig. 9G). Ooid aggregates in the form of compound grapestone intraclasts are also present, and these are >2 mm in diameter and include different coated grains and bioclasts (Fig. 9H). Meniscus (Fig. 10A), peloidal, and micritic cement are the primary diagenetic cement in this microfacies. The rocks of this microfacies are characterized by coarse to very coarse grains carbonate texture with varied sedimentary structures, including planar laminations, wavy laminations, trough cross-bedding (Fig. 10B), ripple forms with cross-lamination (Fig. 10C).

All these observations indicate deposition in high-energy shallow marine conditions, in which the ooids were influenced by the wave and current action (Flugel, 2004). Also, the grainstone texture indicates strong agitated waters and the winnowing of mud. Furthermore, the presence of compound grapestone intraclasts refers to the breaking and reworking in storm-influenced coastal and shallow shelf environments (Scholle and Ulmer-Scholle, 2003). Field observations of cross-bedding, trough cross-bedding, planar laminations, and ripple marks also indicate deposition above the fair-weather wave base. Meniscus cement between the ooids and bioclasts indicates very early diagenetic cementation and meteoric, vadose freshwater diagenesis (Inden and Moore, 1983; Strasser, 1986; Strasser et al., 1995; Flugel, 2004). The association of the ooids with peloids and benthic foraminifera, the marine-phreatic and meteoric cement, and the observed sedimentary structures are indicators that the ooidal microfacies accumulated in oolitic shoal on the sand barrier between the lagoon and the more open water.

4.3. Evaporite lithofacies

Evaporites are an important component within the Fatha Formation, being associated with the carbonates and calcareous mudstones within the cycles. This lithofacies makes up approximately 15 to 43% of the total succession by stratigraphic thickness. The evaporite units overlie the carbonate units in the Fatha cycles. The thickest observed evaporite succession was deposited in the most basinward location. In the formation, two main evaporitic facies are recorded, nodular gypsum (NE) (Fig. 10D) and laminated evaporite (LE) (Fig. 10E), but as a whole, nodular gypsum, comprising chicken-wire (CH) and enterolithic (EN) textures, is more dominant. The thickness of the unit in the Fatha Formation cycles is between 1 and 10 m in the study area. The laminated evaporite is documented in only one cycle across the various sections. The evaporite laminae are typically a few mm in thickness. Where present, the nodules are of variable widths (5-10 mm), and their shapes are typically irregular and rarely elongated or spheroidal. The main evaporite mineral in the outcrops is gypsum, though halite and anhydrite minerals are recorded from the succession in the basin depocentre (Al-Juboury and McCann, 2008). Petrographically, the nodular gypsum comprises chicken-wire structures between the gypsum mineral and mudstone. The laminated evaporite has planar or wavy laminations between gypsum and mudstone. In some cases, dolomite crystals are associated with both the nodular and laminated evaporites.

Nodular evaporite units of the Fatha Formation are stratigraphically associated with the underlying carbonate unit facies and occasionally interfingered with intertidal algal mat bindstones (M8) and stromatolites (M9). The nodular evaporites are then capped by the fluvial siliciclastic deposits (RC). From these observations, it can be concluded that the evaporites may have been developed in a sabkha setting around the basin flanks during arid climate conditions.

The >1 m-thick laminated evaporite facies is recorded in all the studied sections and can be traced for more than 100 km distance. This deposit has been interpreted as representing different parts of evaporitic basins elsewhere, such as Holocene evaporite sequences in the Gulf of Suez, Egypt (Aref et al., 1997), coastal hypersaline pools of the Red Sea (Kushnir, 1981), and Messinian deep-water evaporites of the Mediterranean basin (Ogniben, 1955; Hardie and Eugster, 1971; Garrison et al., 1978). Here, this deposit occurs at the top of a regressive cycle and is interpreted to have

been subaqueously deposited during marine flooding of the evaporitic tidal flats where any depressions were filled with the marine flooding waters.

4.4. Red siliciclastic lithofacies (RC)

This deposit makes up the top of each typical Fatha Formation cycle and comprises 40-78% of the total succession, from the most distal to proximal parts of the studied area. It is comprised of red claystone, red or greyish siltstone, and green or red sandstone. The thickness of the unit is 0.5-6 m in the lower part of the Fatha Formation and 2-8 m in the upper part of the succession. Typical grain size varies from the lower to the upper parts of the formation, with proportions of siltstone and sandstone increasing toward the upper part. The claystone and siltstone are characterized by red color with fine laminations. The presence of planar laminations characterizes the sandstone, cross-bedding, ripple marks (Fig. 10F), flute casts, and load casts. Bioturbation in the form of vertical, horizontal, and inclined burrows increases in the upper part of siltstone and fine sandstone beds; recognized ichnofacies include *Rhyzolithos* (Fig. 10G) and *Skolithos* (Fig. 10H).

Generally, different clastic lithofacies may be differentiated: red claystone (C); laminated red siltstone (LS); cross-bedded sandstone (CS); trough cross-bedded sandstone (TS); rippled sandstone (RS); *Rhyzolithos*-rich sandstone (RhS) and highly bioturbated mudstone-siltstone (HM). The red claystone lithofacies (C) is the most common facies and consists of fine and structureless red claystone. This lithofacies is interbedded with the laminated red siltstone lithofacies (LS), characterized by thin-bedded (0.05 to 0.1 m thick) planar mm-laminated red siltstone. The cross-bedded sandstone (CS) consists of beds of greenish-grey or red sandstone with cross-stratification. In addition, the trough cross-bedded sandstone lithofacies (TS) consists of thick beds (0.5 to 1 m thick) of sandstone with trough cross-stratification. The rippled sandstone lithofacies (RS) is characterized by moderately thick beds (0.3 to 0.4 m thick) of red sandstone with asymmetrical ripple marks (Fig. 10F). The *Rhyzolithos*-rich sandstone (RhS) is characterized by the presence of a large number of root structures on sandstone beds (Fig. 10G), whereas the highly bioturbated mudstone-siltstone (HM) exhibits a high abundance of horizontal and vertical burrows (Fig. 10H).

The red siliciclastic deposits at the top of the cycles are most likely to represent a fluvial system for which sediment was sourced from the adjacent hinterlands of the Zagros Mountains. Moreover, the red siliciclastic claystone and sandstone may indicate fluvio-deltaic deposits sourced from the Zagros Mountains (Aqrawi, 1993). The sandstone lithofacies (CS, TS, and RS) were deposited in higher energy fluvial parts of the system and are most commonly developed in the upper part of the succession. The highly bioturbated mudstone-siltstone lithofacies (HM) and sandstones with *Skolithos,* and *Rhyzolithos* (RhS), which are present in the uppermost part of the succession, indicate shallow-marine, brackish-water deposits (Seilacher, 1967). The evidence for this is the presence of highly abundant horizontal and vertical burrows, and plant root remains.

5. Stratigraphic architecture

A thick succession (50-300 m thick) of the Fatha Formation is preserved in the study areas and is internally characterized by well-developed carbonate-evaporite cycles. The cycles in the marginal parts of the basin are characterized internally by bluish-grey to greenish calcareous mudstone (marl) at their base. This passes up into shallow-marine carbonate deposits that are capped by nodular evaporite deposits (Fig. 11A). In proximal areas considered in this study, continental red-bed siliciclastic units prograded basinward to form the uppermost parts of the individual cycles. The lower boundary of the formation is determined by a change from the underlying highly jointed carbonate rocks of the Jeribe Formation, whereas the upper boundary is gradational with the fluvial depositional cycles of the overlying Injana Formation.

The number of preserved cycles increases from the basin margin towards its depocentre. Between 10 and 40 cycles were identified at each of the study sites based on the presence of evaporite units and overlying flooding surfaces. In the studied sections, completely developed cycles comprise four major units: calcareous mudstone (13-24%), carbonate (5-15%), evaporite (15-43%), and continental red clastic units (40-78%), from the base to the top of each cycle. However, towards the basin depocentre, to the southwest, the preserved facies expression of cycles is more varied and demonstrates that the basin was repeatedly evaporative, such that it accumulated thick gypsum, anhydrite, and halite deposits (Tucker, 1999; Aqrawi et al., 2010).

Significantly, in all the studied sections, the nature of cyclicity changes from the lower to the upper part of the succession in terms of both preserved thickness and internal facies composition. Notably, the proportion of the carbonate and evaporite components is highest in the succession's lower part (Fig, 11B). In contrast, the proportion preserved thickness and grain size of the red continental clastic units that define the uppermost parts of the cycles increase toward the top of the formation (Fig. 11C), and the proportion of marine deposits decreases. The red continental clastic units vary as a percentage of the total formation from the sites closest to the basin margin (78%) to the sites closest to the basin depocentre (40%). Thus, the facies trend of the formation changes from marine dominance in the lower part to a transitional zone in the upper part and then to fluvial dominance in the Injana Formation that overlies the Fatha Formation.

Generally, each cycle and the whole formation have some criteria in common. For example, firstly, both individual cycles and the succession represent a shallowing upward trend that indicates a decrease in water depth. Secondly, each cycle starts with a rapid increase in accommodation space and finish with a decreasing rate of accommodation space generation. This criterion is also seen in the whole formation with high accommodation space generation in the lower part compared with progressively less accommodation space generation toward the upper part.

In this study, the key stratigraphic surface recognized in each cycle is the flooding surface representing a rapid transgression where calcareous mudstones overlie pre-existing red siliciclastic deposits. Above the flooding surface and carbonate mudstones, the cycle typically grades up to shallow water carbonate and then passes up to evaporites. A red fluvial unit then progrades over the evaporite toward the basin. Therefore, each cycle is typically capped by the red fluvial unit at the top, and each cycle represents a regressive and shallowing-upward trend, which progrades toward the basin. The next cycle starts with a new flooding surface.

6. Discussion

The mixed carbonate-evaporite ramp deposits in the proximal areas of the Mesopotamian Basin were subject to dramatic and frequent variations in depositional settings in both time and space. The lower part of the succession is characterized by thick carbonate-evaporite cycles, whereas siliciclastics became dominant toward the upper part of the succession. Overall, this records the

progradation into the basin of siliciclastic detritus of continental origin. This significantly affected carbonate production and evaporites precipitation.

In the lower part of the formation, each cycle typically passes from a calcareous mudstone unit (marl) at its base, to a shallowing-up carbonate unit, to a nodular evaporite unit, which is itself capped by a red continental clastic unit. These facies trend changes in the upper part of the succession where the marine units are thinner. Here, evaporite deposits are missing, and carbonate units are typically only 0.2 to 0.5 m thick. Moreover, the red continental clastic unit becomes thicker (5 to 10 m) in the upper part of the succession. (Figure 12).

The calcareous mudstone units (CM) in the lowermost parts of each cycle were deposited in a laterally extensive low-energy hypersaline lagoon, as demonstrated by the occurrence of hypersaline benthic foraminifera (rotaliids and miliolids) and ostracods. This depositional setting became progressively shallower through time toward the upper part of the succession. At the same time, more normal marine conditions developed, as demonstrated by the abundant occurrence of stenohaline organisms (Bryozoa), oysters, and marine-brackish water ichnofacies (*Skolithos*).

Based on the interpreted microfacies, each cycle's carbonate sediments were deposited in various environments along the basin margin, including low- and high-energy hydrodynamic settings. The detailed microfacies thus represent lateral variations in the extent and morphology of the lagoonal complexes developed on the basin margin. The length scale of these variations was less than the spacing of the measured sections, as it is not consistently possible to trace individual microfacies from one section in any one cycle to the equivalent cycle in an adjacent section. The supposed depositional model of this lateral variation in lagoonal and near-shore environments at a scale of tens of kilometers is depicted in Figure 12.

The skeletal mudstone, wackestone, and packstone microfacies (M1-M3) at the base of the carbonate units represent deposits of restricted hypersaline lagoons as evidenced by the presence of restricted foraminifera (rotaliids and miliolids) and ostracods with evaporite pseudomorphs that indicate hypersalinity. In contrast, the predominate of algal laminites, stromatolites, and dolostone indicates deposition in an intertidal depositional setting represented by a group of microfacies (M4-

M10). Deposition of high-energy carbonate microfacies of M16 represents the presence of ooidal grainstone in sand shoals.

The evaporite sediments at the top of the carbonates represented regressive facies and were deposited in various environments. The main abundant evaporite facies is of a nodular type, including chicken-wire (CH) and enterolithic (EN) evaporites resulting from deposition in a coastal sabkha (Warren and Kendall, 1985; Warren, 2006). Such nodular evaporites originate from repeated arid and high rainfall episodes when the original gypsum crystals formed within the capillary groundwater zone undergo repeated hydration and dehydration (Schreiber and Tabakh, 2000). Laminated evaporites (LE) were subaqueously deposited during flooding over the tidal flat. The presence of evaporite deposits indicative of emergence at the basin margin contrast markedly with the model proposed previously for this basin based on the recognition solely of subaqueous evaporites from basin-depocentre settings, where thick laminated selenite and halite deposits are identified (Al-Juboury and McCann, 2008).

The initial accumulation of siliciclastic deposits derived from the hinterlands during the Miocene occurred during deposition of the Fatha Formation when the red clastic units started prograding south-westward into the basin. Concomitant shoreline migration into the basin through time is represented by the overall variation in thickness of the preserved succession from the basin margin to its depocentre: a thinner succession comprising fewer cycles is recorded at the basin margin. In addition, siliciclastic-dominated cycles are preserved around the basin margin, and evaporite-dominated cycles were best developed in the basin depocentre. The presence of climatically wet hinterlands and significant fluvial activity around the basin margin and its late-stage progradation towards the basin depocentre eventually resulted in a progressive termination of evaporite deposition, from a basin-margin to a basin-depocentre setting, over time.

Several factors influenced sedimentation rates and the position of the shoreline through time. The Oligocene-Miocene records several climatic fluctuations or warm spikes and sea-level rises, and basin margin sequence architectures were primarily controlled by glacio-eustatic sea-level changes (Kominz, 2001; Miller et al., 2005), including in the studied area. The deposition of the Miocene Fatha Formation recorded an excellent example of the Miocene climatic fluctuations. Furthermore, the presence of a mid-Miocene Climatic Optimum, which lasted from the middle Burdigalian to the

Langhian (Miller et al., 1991), was contemporaneous with the deposition of evaporite-carbonate deposits of the Fatha Formation. Moreover, reduced evaporite deposition and increased fluvial activity from the basin margin through time – illustrated by coastal progradation – may also have been driven by an overall climate change from relatively arid to relatively more humid. The high-frequency carbonate-evaporite-clastic cycles in the current study extend to Syria and Iran and are continuous over about 2000 km and are well preserved throughout the entire basin. The cycles are traceable for tens of kilometers, this distance usually only being limited by outcrop continuity. This is a possible evidence for orbital forcing having a control on the basin stratigraphy. Other strong evidence of orbital forcing and eustatic control is the regularity and correlation of the cycles across the region. Also, the cycles were wholly preserved in the basin-depocentre, whereas toward the basin-margin, not all cycles are preserved due to onlapping. As a result, 10 to 40 cycles were recorded in the basin-margin, whereas 50 cycles were documented in the basin-depocentre (Tucker, 1999). By dividing the total duration of the formation (3.0Myr, (Abdullah, 2016)) by the number of cycles in the basin-depocentre (50), a mean cycle duration of 60Kyr is obtained. These values fall in the vicinity of the ' 'Earth's short eccentricity cycle that is modulated in the range from 95 to 123 k.y. (Berger, 1977). This means that a mix of obliquity and eccentricity-forced cycles are probably being expressed. Overall, the progradation of the siliciclastic wedge progressively replaced carbonate-evaporite sedimentation in the basin and changed the system to an overfilled fluvial basin by the late stages of Fatha deposition, after which fluvial facies of the overlying Injana Formation became dominant.

Tectonically, the position of the Miocene foreland basin meant that it was subjected to collisional forces between the Arabian and Eurasian plates. Increasing siliciclastic supply during the middle Miocene would have resulted from erosion of the uplifted areas of the developing fold and thrust belt. The first appearance of the siliciclastic deposits during the deposition of the Fatha Formation was a signal of initiation of the early stage of continent-continent collision (Al-Qayim et al., 2012). Indeed, the shallowing-upward trend of the Fatha Formation is typical of foreland-basin fills, indicating the significance of tectonic setting on basin stratigraphy (Baars and Stevenson, 1982; Sami and James, 1994; Brown, 2002). A high rate of sediment supply outpaced the generated accommodation space across the basin and terminated the carbonate factory. Hence, tectonics and sediment supply determined accommodation in the basin and collectively acted to determine the overall progradational geometry of the formation. Autocyclic processes of sabkha progradation and migration of shoreline toward the basin could also have been contributed. In addition, the

reactivation of vertical block movements in Iraq during the Miocene influenced the lateral variations and the repetition of the deposits (Bahroudi and Koyi, 2004; Sissakian et al., 2016). This is evidenced by the presence of Mosul High between the Sinjar and Kirkuk subbasins (Fig. 5B).

Similar sedimentological characterizations of carbonate, evaporite, and siliciclastic to middle Miocene Fatha Formation have been investigated in many modern and ancient basins (Kendall and Patrick, 1969; Wood and Wolfe, 1969; Alsharhan et al., 1995; Alsharhan and Kendall, 2003). In particular, a similar mode of deposition can be observed between the middle Miocene Fatha Formation and the modern sabkha cycles in the Arabian Gulf (Persian Gulf). The Gulf is located between the northeastern Arabian Peninsula and Zagros mountains in Iran and extends 1000 km in length and 200-300 km wide. An idealized landward section passes in order through open-marine skeletal deposits, oolitic belts, lagoons, intertidal, and ends with supratidal sabkha evaporites (Warren and Kendall, 1985). These lateral and vertical distributions in the facies are analogous to the middle Miocene Zagros foreland basin. Moreover, there is a close link between the Neogene foreland basin of the Arabian Plate and the modern Zagros foreland basin (Pirouz et al., 2011). The vertical Neogene succession has an active modern-day equivalent, where one passes from carbonate ramp and sabkha deposits along the Arabian Gulf, equivalent to Fatha/Gachsaran Formation, to shallow marine clastic sediment along the northern part of the Gulf, equivalent to Guri Formation in Iran, to meandering rivers close to the coast, equivalent to Injana/Agha Jari Formation, and finally to braided rivers in the Zagros mountains that represent Mukdadiya and Bai Hassan/Bakhtyari formations.

7. Conclusions

The studied carbonate-evaporite succession is important because it provides a detailed paleoenvironmental record of the development and infill of the Zagros foreland basin. Additionally, the succession is significant in terms of its role as a petroleum system; it is of considerable economic importance. The Miocene carbonate-evaporite succession of the Fatha Formation is predominantly of marine origin and was deposited across a very low-angle, inclined ramp setting in which inner-ramp facies are detailed in this study. Deposits are arranged into a series of 10 to 40 shallowing-upward cycles. The main deposit divisions within each cycle are calcareous mudstones, carbonates, evaporites, and red siliciclastic deposits. A marine flooding

surface caps each cycle. Each preserved depositional cycle has a facies arrangement which in the lower part is indicative of low-energy calcareous mudstone accumulation and passes up to moderate- to high-energy shallow marine carbonates or low-energy lagoonal carbonates. They are, in turn, overlain by nodular evaporites and, in some cases, are capped by a red siliciclastic unit at the top of the cycle.

Based on the microfacies analysis, different carbonate environmental settings are recognized along the basin margin. Significant variability is evident over length scales of tens of kilometers. Shoreline deposits range from high-energy rippled and cross-bedded carbonate grainstones to low-energy stromatolite facies of protected embayment in a complex and laterally extensive lagoonal system.

The formation overall records a progradational shallowing-upward succession. The preserved facies trend through the succession can be regarded as being due to a combination of variations in sea level, salinity, climate, carbonate-evaporite production, siliciclastic supply, tectonic subsidence rate, and tidal flat progradation. The cycles can be traced and correlated regionally along with the NW-SE trend of the foreland basin. The overall up-succession variation in facies was driven by increasing siliciclastic supply from the uplifting Zagros Mountains due to the collision between the Arabian and Iranian plates. As a result, a siliciclastic alluvial depositional system advanced into the basin, causing regression of the shoreline.

Acknowledgments

The Ministry of High Education of Kurdistan Regional Government (KRG) provided funding for this research. Dr. Kamal Haji Karim is thanked for his help in the field and valuable advice.

References

Abdullah, H., Collier, R., Mountney, N., 2019. The palaeoshoreline of Early Miocene formations (Euphrates and Jeribe) at the periphery of the Zagros Foreland Basin, Sulaimani governorate, Kurdistan region, NE Iraq. Arabian Journal of Geosciences 12, 1-15.

Abdullah, H.G., 2016. Variations in cyclical carbonate-evaporite depositional architectures. University of Leeds, UK, Unpublished PhD, p. 299.

Abou-Ouf, M., Durgaprasada Rao, N., Taj, R., 1988. Benthic foraminifera from littoral sediments of Al Lith-Al Qunfidhah coast, southeastern Red Sea. Indian Journal of Marine Sciences 17, 217-221.

Ajel, M., 2004. Sedimentology of the transitional zone of non-marine deposits in the Fatha Formation (Middle Miocene) in selected sections in N and NW of Iraq. University of Baghdad, Iraq. MSc thesis, p. 150.

Al-Juboury, A.I., McCann, T., 2008. The Middle Miocene Fatha (Lower Fars) formation, Iraq. GeoArabia 13, 141-174.

Al-Qayim, B., Omer, A., Koyi, H., 2012. Tectonostratigraphic overview of the Zagros suture zone, Kurdistan region, Northeast Iraq. GeoArabia 17, 109-156.

Al-Rawi, Y.T., Sayyaeb, A.S., Jassim, J.A., Tamar-Agha, M., Al-Sammarai, A.I., Karim, S.A.B., M.A. , Dhiab, S.H., Faris, F.M., Anwar, F., 1993. New names for some of the late Early Miocene-Pliocene formations of Iraq (Fatha, Injana, Mukdadiya and Bai-Hassan Formations). Iraqi Geological Journal 25, 1-18.

Alsharhan, A., Kendall, C.S.C., Whittle, G., 1995. Holocene carbonate evaporites of Abu Dhabi, United Arab Emirates-field trip guidebook. IGCP-349, United Arab Emirates University, Al Ain.

Alsharhan, A.S., Kendall, C.G.S.C., 2003. Holocene coastal carbonates and evaporites of the southern Arabian Gulf and their ancient analogues. Earth-Science Reviews 61, 191-243.

Ameen, B.M., Karim, K.H., 2007. Evidence of tempestite and possible turbidite in the middle Miocene lagoonal deposits of Lower Fars Formation, Kurdistan region, NE Iraq, in: Sadek, A. (Ed.), The second International Conference of Geo-resource of the Middle East and North Africa. Geo-resource of the Middle East and North Africa, Cairo University, Egypt, pp. 745-756.

Amirshahkarami, M., 2013. Microfacies correlation analysis of the Oligocene-Miocene Asmari Formation, in the central part of the Rag-e-Safid anticlinal oil field, Zagros Basin, southwest Iran. Turkish Journal of Earth Sciences 22, 204-219.

Amirshahkarami, M., Vaziri-Moghaddam, H., Taheri, A., 2007. Sedimentary facies and sequence stratigraphy of the Asmari Formation at Chaman-Bolbol, Zagros Basin, Iran. Journal of Asian Earth Sciences 29, 947-959.

Aqrawi, A.A.M., 1993. Miocene evaporitic sequence of the southern Mesopotamian Basin. Marine and Petroleum Geology 10, 172-179.

Aqrawi, A.A.M., Horbury, A., Sadooni, F., 2010. The Petroleum Geology of Iraq. Wiley, Beaconsfield, UK, pp.424.

Aref, M.A., Attia, O.E., Wali, A.M., 1997. Facies and depositional environment of the Holocene evaporites in the Ras Shukeir area, Gulf of Suez, Egypt. Sedimentary Geology 110, 123-145.

Baars, D., Stevenson, G., 1982. Subtle stratigraphic traps in Paleozoic rocks of Paradox basin, in: Halbouty, M.T. (Ed.), The Deliberate Search for the Subtle Trap. The American Association of Petroleum Geologists, Memoir 32, pp. 131-158.

Bahroudi, A., Koyi, H.A., 2004. Tectono-sedimentary framework of the Gachsaran Formation in the Zagros foreland basin. Marine and Petroleum Geology 21, 1295-1310.

Becker, F., Bechstädt, T., 2006. Sequence stratigraphy of a carbonate-evaporite succession (Zechstein 1, Hessian Basin, Germany). Sedimentology 53, 1083-1120.

Berger, A., 1977. Support for the astronomical theory of climatic change. Nature 269, 44-45.

Boersma, A., 1978. Foraminifera, in: Haq, B.U., Boersma, A. (Eds.), Introduction to Marine Micropaleontology. Elsevier, New York, pp. 19-77.

Boltovskoy, E., Wright, R., 1976. Recent foraminifera. W. Junk, Netherlands., pp.515.

Bradshaw, J., 1961. Laboratory experiments on the ecology of foraminifera. Contributions from the Cushman Foundation for Foraminiferal Research 12, 87-106.

Brown, A.L., 2002. Outcrop to Subsurface Stratigraphy of the Pennsylvanian Hermosa Group Southern Paradox Basin USA. West Virginia University, PhD thesis, p. 181.

Buday, T., 1980. Regional Geology of Iraq: Stratigraphy and Paleogeography. Dar Al-Kutub, Mosul, Iraq, pp.445.

Buday, T., Jassim, S.Z., 1987. The Regional geology of Iraq. 2: Tectonic, Magmatism and Metamorphism. Geological Survey and Mineral Investigation, Baghdad, Iraq, pp.492.

Burchette, T., Wright, V., 1992. Carbonate ramp depositional systems. Sedimentary Geology 79, 3-57.

Busk, H.G., Mayo, H.T., 1918. Some notes on the geology of the Persian oilfields. Institution of petroleum technologists

Carozzi, A.V., 1961. Distorted oolites and pseudoolites. Journal of Sedimentary Petrology 31, 262–274.

Debenay, J.-P., Geslin, E., Eichler, B.B., Duleba, W., Sylvestre, F., Eichler, P., 2001. Foraminiferal assemblages in a hypersaline lagoon, Araruama (RJ) Brazil. Journal of Foraminiferal Research 31, 133-151.

Dunham, R.J., 1962. Classification of carbonate rocks according to depositional textures, in: Ham, W.E. (Ed.), Classification of Carbonate Rocks. Memoir of the American Association of Petroleum Geologists, Tulsa, pp. 108-121.

Dunnington, H.V., 1958. Generation, migration, accumulation, and dissipation of oil in northern Iraq: Middle East, in: weeks, L.G. (Ed.), Habitat of oil. American Association of Petroleum Geologists, Tulsa, Oklahoma, USA, pp. 1194-1251.

Embry, A.F., Klovan, J.E., 1971. A Late Devonian reef tract on northeastern Banks Island, NWT. Bulletin of Canadian Petroleum Geology 19, 730-781.

Flugel, E., 2004. Microfacies of Carbonate Rocks: Analysis, Interpretation and Application. Springer-Verlag, Berlin, pp.984.

Garrison, R., Schreiber, B., Bernoulli, D., Fabricius, F., Kidd, R., Melieres, F., 1978. Sedimentary petrology and structures of Messinian evaporitic sediments in the Mediterranean Sea, Leg 42A, Deep Sea Drilling

Project, in: Hsu, K., Montadert, L. (Eds.), Initial Reports of the Deep Sea Drilling Project. U.S. Government Printing Office, Washington, pp. 571-612.

Geel, T., 2000. Recognition of stratigraphic sequences in carbonate platform and slope deposits: empirical models based on microfacies analysis of Palaeogene deposits in southeastern Spain. Palaeogeography, Palaeoclimatology, Palaeoecology 155, 211-238.

Gertsch, B., Keller, G., Adatte, T., Berner, Z., Kassab, A., Tantawy, A., El-Sabbagh, A., Stueben, D., 2010. Cenomanian–Turonian transition in a shallow water sequence of the Sinai, Egypt. International Journal of Earth Sciences 99, 165-182.

Ghafur, A., 2012. Sedimentology and reservoir characteristics of the Oligocene-Early Miocene carbonates (Kirkuk Group) of southern Kurdistan. Cardiff University, PhD Thesis, p.

Gheith, A.G., Auf, M.A.A., 1996. Textural characteristics, mineralogy and fauna in the shore zone sediments at Rabigh and Sharm Al-Kharrar, eastern Red Sea, Saudi Arabia. Journal of King Abdulaziz University: Marine Sciences 7, 1-2.

Ghosh, A.K., Sarkar, S., 2013. Facies analysis and paleoenvironmental interpretation of Piacenzian carbonate deposits from the Guitar Formation of Car Nicobar Island, India. Geoscience Frontiers 4, 755-764.

Gill, W.D., Ala, M.A., 1972. Sedimentology of Gachsaran Formation (lower Fars series), Southwest Iran. American Association of Petroleum Geologists Bulletin 56, 1965-1974.

Goff, J.C., Jones, R.W., Horbury, A.D., 1995. Cenozoic basin evolution of the northern part of the Arabian Plate and its control on hydrocarbon habitat, Middle East Petroleum Geosciences, GEO94, Bahrain, pp. 402-412.

Grabowski, G.J., Liu, C., 2009. Ages and Correlation of Cenozoic Strata of Iraq, International Petroleum Technology Conference. International Petroleum Technology Conference, Doha, Qatar.

Grabowski, G.J., Liu, C., 2012. Age, Correlation, Depositional Environments, and Sedimentary History of the 'Fat'ha Formation (Burdigalian, Lower Miocene) of Iraq, GEO 2012.

Hamid, S.F., 1994. Sedimentological studies of Fatha Formation in sheikh Ibrahim and Butmah anticlines, SW Iraq. University of Mosul, Iraq. MSc thesis, p. 140.

Haq, B.U., Boersma, A., 1998. Introduction to marine micropaleontology. Elsevier, Singapore, p. 367.

Hardie, L.A., Eugster, H.P., 1971. The depositional environment of marine evaporites: a case for shallow, clastic accumulation. Sedimentology 16, 187-220.

Hariri, M.S., 2008. Effect of hydrographic conditions on the ecology of benthic foraminifera in two different hypersaline lagoons, eastern Red Sea coast, Kingdom of Saudi Arabia. Journal of King Abdulaziz University: Marine Sciences 19, 3-13.

Hudson, J., 1963. The recognition of salinity-controlled mollusk assemblages in the Great Estuarine Series (Middle Jurassic) of the Inner Hebrides. Palaeontology 6, 318-326.

Inden, R.F., Moore, C.H., 1983. Beach Environment, in: Scholle, P.A., Bebout, D., Moore, C. (Ed.), Carbonate depositional environments. The American Association of Petroleum Geologists, Oklahoma, pp. 212-240.

James, G.A., Wynd, J.G., 1965. Stratigraphic nomenclature of Iranian oil consortium agreement area. American Association of Petroleum Geologists Bulletin 49, 2182-2245.

Jassim, S.Z., Goff, J.C., 2006. Geology of Iraq, First ed. Dolin, Praque and Moravian Museum, Brno, Zelny trh 6, Brno, Czech Republic, pp.341.

Karim, K.H., 2010. Modification of the time-expanded stratigraphic column of north east Iraq. Petroleum geology of Iraq, Baghdad Abstract Book, 4.

Kendall, C.G.S.C., Alsharhan, A.S., Cohen, A., 2002. The Holocene tidal flat complex of the Arabian Gulf coast of Abu Dhabi, in: Boer, B., Barth, H.J. (Eds.), The sabkhas of the Arabian Peninsula Region: Distribution and ecology. Kluwer Academic Publishers, Dordrecht, pp. 21-35.

Kendall, C.G.S.C., Patrick, A., 1969. Holocene shallow-water carbonate and evaporite sediments of Khor al Bazam, Abu Dhabi, southwest Persian Gulf. AAPG Bulletin 53, 841-869.

Kharajiany, S., 2008. Sedimentary facies of Oligocene rock units in Ashdagh mountain—Sangaw district—Kurdistan region, NE Iraq. University of Sulaimani, MSc Thesis, p. 107.

Kinsman, D.J., Park, R.K., 1976. Algal belt and coastal sabkha evolution, Trucial Coast, Persian Gulf, in: Walter, M.H. (Ed.), Stromatolites. Developments in Sedimentology, pp. 421-433.

Kominz, M., 2001. Sea level variations over geologic time. Encyclopedia of Ocean Sciences, 2605-2613.

Kushnir, J., 1981. Formation and early diagenesis of varved evaporite sediments in a coastal hypersaline pool. Journal of Sedimentary Research 51, 1193-1203.

Mahmoodabadi, R.M., 2020. Facies analysis, sedimentary environments and correlative sequence stratigraphy of Gachsaran Formation in SW Iran. Carbonates Evaporites 35.

Marandi, M., Jahani, D., Uromeihy, A., Reihan, M. K., 2019. Analysis of structure and textures of anhydrite mineral in Gachsaran Formation in Gotvand area, Iran. Open Journal of Geology 7.

Miller, K.G., Feigenson, M.D., Wright, J.D., Clement, B.M., 1991. Miocene isotope reference section, Deep Sea Drilling Project Site 608: an evaluation of isotope and biostratigraphic resolution. Paleoceanography 6, 33-52.

Miller, K.G., Kominz, M.A., Browning, J.V., Wright, J.D., Mountain, G.S., Katz, M.E., Sugarman, P.J., Cramer, B.S., Christie-Blick, N., Pekar, S.F., 2005. The Phanerozoic record of global sea-level change. science 310, 1293-1298.

Mohamed, M., Madkour, H., El-Taher, A., 2013. Recent benthic foraminifera in the saline pool and its surrounding areas at Ras Shuukier and Gulf of Suez, Egypt. Indian Journal of Geo-Marine Sciences 42, 293-299.

Murray, J.W., 1973. Distribution and ecology of living benthic foraminiferids, New York, Crane, Russak, pp.274.

Ogniben, L., 1955. Inverse graded bedding in primary gypsum of chemical deposition. Journal of Sedimentary Petrology 25, 273-281.

Pirouz, M., Simpson, G., Bahroudi, A., Azhdari, A., 2011. Neogene sediments and modern depositional environments of the Zagros foreland basin system. Geological Magazine 148, 838-853.

Sami, T.T., James, N.P., 1994. Peritidal carbonate platform growth and cyclicity in an early Proterozoic foreland basin, upper Pethei Group, northwest Canada. Journal of Sedimentary Research 64, 111-131.

Schmitt, W.L., 1957. Barnacles, in: Laad, H.S. (Ed.), Treatise on Marine Ecology and Paleoecology. Geological Society of America Memoir, pp. 1158-1159.

Scholle, P.A., Ulmer-Scholle, D.S., 2003. A Color Guide to the Petrography of Carbonate Rocks: Grains, Textures, Porosity, Diagenesis. American Association of Petroleum Geologists Memoir 77, Tulsa, Oklahoma, U.S.A, pp.459.

Schreiber, B.C., Tabakh, M.E., 2000. Deposition and early alteration of evaporites. Sedimentology 47, 215-238.

Seilacher, A., 1967. Bathymetry of trace fossils. Marine Geology 5, 413-428.

Sharland, P.R., Archer, R., Casey, D.M., Davies, R.B., Hall, S.H., Heward, A.P., Horbury, A.D., Simmons, M.D., 2001. Arabian Plate Sequence Stratigraphy. GeoArabia Special Publication 2, Gulf PetroLink, Bahrain, pp.371.

Shawkat, M.G., 1979. The sedimentology of the Lower Fars Formation (Miocene) of Northern Iraq. University of Newcastle Upon Tyne, UK. PhD, p.

Shawkat, M.G., Tucker, M.E., 1978. Stromatolites and sabkha cycles from the Lower Fars Formation (Miocene) of Iraq. Geologische Rundschau 67, 1-14.

Sissakian, V., Karim, S., Al-Kubaisy, K., Al-Ansari, N., Knutsson, S., 2016. The Miocene sequence in Iraq, a review and discussion on the stratigraphy, paleogeography and economic potential. Journal of Earth Sciences and Geotechnical Engineering 6, 271-317.

Soleimani, B.a.B., A., 2015. The Miocene Gachsaran Formation evaporite cap rock, Zeloi oil field, SW Iran. Carbonates and Evaporites 30, 287-306.

Strasser, A., 1986. Ooids in Purbeck limestones (lowermost Cretaceous) of the Swiss and French Jura. Sedimentology 33, 711-727.

Strasser, A., Arnaud, H., Baudin, F., Röhl, U., 1995. Small-scale shallow-water carbonate sequences of Resolution Guyot (Sites 866, 867, and 868): Northwest Pacific atolls and guyots, in: Winterer, E.L., Sager, W. W., Firth, J. V., and Sinton, J. M. (Ed.), Proceeding of the Ocean Drilling Program, Scientific Results, College Station, Texas, pp. 119-131.

Thrana, C., Talbot, M.R., 2006. High-frequency carbonate-siliciclastic cycles in the Miocene of the Lorca Basin (Western Mediterranean, SE Spain). Geologica Acta 4, 343-354.

Tucker, M.E., 1999. Sabkha cycles, stacking patterns and controls: Gachsaran (Lower Fars/Fatha) Formation, Miocene, Mesopotamian Basin, Iraq. Neues Jahrbuch fur Geologie und Palaontologie-Abhandlungen 214, 45-69.

Tucker, M.E., Wright, V.P., 1990. Carbonate Sedimentology. Blackwell Scientific Publications, Oxford, UK, pp.482.

van Bellen, R.C., Dunnington, H.V., Wetzel, R., Morton, D.M., 1959. Lexi Stratigra Interna, III, Asie, Iraq. Centre National de la Recherche Scientifique, Paris, pp.337.

Vaziri-Moghaddam, H., Seyrafian, A., Taheri, A., Motiei, H., 2010. Oligocene-Miocene ramp system (Asmari Formation) in the NW of the Zagros basin, Iran: microfacies, paleoenvironment and depositional sequence. Revista Mexicana de Ciencias Geológicas 27, 56-71.

Warren, J.K., 2006. Evaporites: Sediments, Resources and Hydrocarbons. Springer Science & Business Media, Brunei, pp.1035.

Warren, J.K., Kendall, C.G.S.C., 1985. Comparison of sequences formed in marine sabkha (subaerial) and salina (subaqueous) settings--modern and ancient. American Association of Petroleum Geologists Bulletin 69, 1013-1023.

Wood, G., Wolfe, M., 1969. Sabkha cycles in the Arab/Darb formation off the Trucial Coast of Arabia. Sedimentology 12, 165-191.

Wright, V., 1986. Facies sequences on a carbonate ramp: the Carboniferous Limestone of South Wales. Sedimentology 33, 221-241.

Ziegler, M.A., 2001. Late Permian to Holocene paleofacies evolution of the Arabian Plate and its hydrocarbon occurrences. GeoArabia 6, 445-504.

Table Captions

Table 1. Geographic coordinates of the studied sections.

Table 2. Descriptions and interpretations of the carbonate microfacies in the Fatha Formation.

Figure Captions

Figure 1. Geological maps of the study area. (A) Geological map of the study area, showing the locations of the studied outcrop sections. (B) Structural map of northern Iraq, including Kurdistan structural elements and the study area (Aqrawi et al., 2010).

Figure 2. The graphic sedimentary sections recorded from the Fatha Formation in the studied sections. Black ticks denote where samples were taken.

Figure 3. Summary of the main stratigraphic units exposed in the studied areas. The Fatha Formation forms the middle Miocene deposit, which is widely exposed.

Figure 4. Chronostratigraphic column of the studied basin in Iraq from late Oligocene to Recent, after (Karim, 2010).

Figure 5. Palaeogeographic map of the middle Miocene basin. (A) Palaeogeographic map of the Arabian Plate, illustrating the distribution of the sedimentary facies of the middle Miocene units (Sharland et al., 2001). (B) Palaeogeographic map of the Fatha Formation in Iraq (Goff et al., 1995). Two main depocentres were developed in Iraq, including the Sinjar sub-basin that extended to Syria and Zagros (Mesopotamian) sub-basin that extended to Iran, where Gachsaran Formation was deposited.

Figure 6. Representative Scanning Electron Microscope images of extracted microfossils from calcareous mudstone units (CM): (A, B) Variations in size of two different species of *Ammonia*. (C, D) Two different species of ornamented ostracods with different sizes. (E, F) Different specimens of miliolids. (G) A bryozoa specimen from the upper part of the succession. (H): A gastropod specimen from the upper part of the succession.

Figure 7. Representative photomicrographs of the Fatha Formation. Calcareous mudstone facies (CM): **(A)** Increased quartz grain content (the white grains) toward the top of a calcareous mudstone unit in muddy matrix with benthic foraminifera (the red arrow). Carbonate microfacies: (B) Quartz mudstone microfacies in a micro-sparite matrix (M1). (C) Rotaliid wackestone microfacies (M2). (D) Miliolid wackestone microfacies (M3). (E) Highly micritized skeletal packstone microfacies (M4) showing unidentified micritized bioclasts (the white arrow) and a miliolid (the red arrow) in a muddy matrix. (F) Bioclastic gastropod-bivalve packstone microfacies (M5). (G, H) Laminated pellet grainstone microfacies (M7) pass up from dark grey laminated sandy carbonate to light grey laminae of pelleted grainstone microfacies.

Figure 8. Representative photomicrographs of the Fatha Formation. Carbonate microfacies: (A) Bioclastic barnacle-oyster floatstone microfacies (M6). (B) Algal bindstone microfacies (M8). (C, D) Thin laminae of laminated mudstone microfacies (M8) and short exposure surfaces (the blue arrow), possibly reflecting tidal rhythms. (E, F) Stromatolites (M9) (the blue arrow), fenestrate algal bindstone (M8) (the black arrow), and a thin exposure surface at the top (the red arrow). (G) Dolo-mudstone microfacies (M10), including fine dolomite crystals. (H) Echinoid packstone microfacies (M11).

Figure 9. Representative photographs of the Fatha Formation. Carbonate microfacies: (A) Bioclastic peloidal grainstone microfacies (M12). (B) Bivalve rudstone microfacies (M13). (C) Slightly rippled carbonate surface with bivalves in bivalve rudstone microfacies (M13). (D) Peloidal-ooidal grainstone microfacies (M14). (E) Bioclastic calc-arenite microfacies (M15), including rotaliids (the blue arrows). (F) Ripple mark in bioclastic calc-arenite microfacies (M15). (G) Ooidal packstone to grainstone microfacies (M16). (H) Ooidal grainstone microfacies (M16).

Figure 10. Field photographs from the Fatha Formation: Carbonate facies: (A) Ooidal grainstone microfacies (M16). (B) Trough cross bedding from ooidal grainstone microfacies (M16). (C) Ripple marks from ooidal grainstone microfacies (M16). Evaporite facies: (D) Nodular evaporite facies with chicken-wire structure (CH). (E) Laminated to folded evaporites between gypsum and mudstone laminae (LE). Clastic facies: (F) Ripple marks on the surface of a sandstone bed from the upper part of the formation (RS). (G) Continental sandstone from the upper part of the formation with *Rhyzolithos* (RhS). (H) Highly bioturbated bluish-red mudstone-siltstone (HM) from the upper part of the formation with vertical *Skolithos* and horizontal burrows.

Figure 11. Representative field photographs of Fatha cycles. (A) Field photograph of an individual cycle of the Fatha Formation. (B) A field photograph of the lower part of the succession shows the carbonate-evaporite-dominated cycles in the Darbandikhan area. (C) A field photograph of the upper part of the succession shows red siliciclastic-dominated cycles in the Sangaw area.

Figure 12. Depositional model of the middle Miocene Fatha Formation at the periphery of the Zagros foreland basin, (A) Regional-scale depositional model, including sedimentary facies palaeoenvironments, facies associations, and progradational stacking of facies. (B, C, and D) Representative summary log sections in the proximal, medial, and distal shallowing-upward cycles. Siliciclastic input from the hinterlands outpaced the marine deposits and prograded toward the basin. (E) Architectural block diagram of restricted and hypersaline lagoons that separated from the open marine by carbonate shoals. (F) Architectural block diagram of supratidal succession.

Table 1: Geographic coordinates of the studied sections**.**

Sections	Thickness (m)	Latitude N	Longitude E	Structure	Desc
Basara	195	35° 26′ 40.30″	45° 09′ 25.84″	Basara Gorge	26 km SW
Takiya	245	35° 39′ 07.38″	44° 57′ 28.90″	Qishlagh	45 km NW
Krbchna	116	35° 17′ 53.65″	45° 16′ 22.31″	Sargrma	32 km SW
Darbandikhan	148	35° 06′ 43.01″	45° 42′ 12.07″	Darbandikhan	53 km SE
Chnarah	50	35° 08′ 37.78″	45° 41′ 24.05″	Darbandikhan	45 km SE
Aj Dagh	182	35° 09′ 31.87″	45° 17′ 50.98″	Aj Dagh	18 km SE
Sangaw	171	35° 16′ 39.26″	45° 09′ 49.63″	Qara-Wais	1 km SW
Mamlaha	300	35° 22′ 06.84″	45° 00′ 27.72″	Qara-Wais	19 km NW
Kfri	120	34° 42′ 04.83″	44° 57′ 53.07″	Bawa-Shaswar	69 km S S

Click here to access/download;Table;Table 2.docx

1.1 Table 2: Descriptions and interpretations of the carbonate microfacies in the Fatha Formation

Microfacies	Description	Physical structures and geometries	Interpretation	Figures
1. Low-energy restricted hypersaline lagoon facies association				
Mudstone (M1)	M1a: Bioturbated mudstone sub-microfacies: lime mud matrix, ostracods and miliolids.	Highly bioturbated mud and very fine-grained texture, non-laminated and structureless.	Low-energy restricted hypersaline lagoon. Inner ramp.	
	M1b: Quartz mudstone sub-microfacies: Mud to micro sparite matrix. 20-30% of quartz and chert grains with oysters, ostracods, miliolids and echinoid plates and spines.	Thin beds (10-40cm thick) with planar and wavy laminations.	Mixed siliciclastic-carbonate coastal environment. Inner ramp.	7B
Rotaliids wackestone (M2)	Lime mud and local micro sparite matrix. Rotaliids (10-30%), ostracods, miliolids and few barnacles. Quartz, chert and evaporite pseudomorphs.	Beds between 20 and 40cm thick. Bioturbations.	Low energy hypersaline restricted lagoon. Inner ramp.	7C
Miliolids wackestone (M3)	Lime mud matrix, miliolids (10%), ostracods and rotaliids. Micritized unidentified bioclasts.	Beds between 20 and 50cm thick. Bioturbations and micritization.	Low energy restricted lagoon. Inner ramp.	7D
2. Shallow lagoon to intertidal facies association				
Strongly Micritized bioclastic packstone (M4)	Bioturbated mud matrix, unidentified Micritized bioclasts with few ostracods and miliolids.	Beds between 10 and 30cm thick with highly bioturbations.	Low energy and well oxygenated lagoon to intertidal. Inner ramp.	7E
Bioclastic gastropods-bivalves packstone (M5)	Micrite matrix. 50-60% gastropods and bivalves. Minor components: echinoids, bryozoas, miliolids, rotaliids and serpulids. Quartz and chert grains. The bivalve shells have been subjected to micritization and dissolution.	This lithofacies is characterized by a very coarse-grained texture, massive beds (40-50cm thick). Micritic intraclasts and micritic envelopes are present.	Low energy shallow lagoon. Inner ramp.	7F

Oyster-barnacles floatstone (M6)	Mud and local sparite matrix. Oysters (>2mm), barnacles (>2mm), bivalves, serpulids, echinoids and bryozoas. Quartz and chert grains.	The lithofacies is characterized by massive fossiliferous beds (30 to 50cm thick) and very coarse-grained texture with large oyster and barnacles.	Low energy and low salinity conditions. Shallow lagoon to intertidal settings. Inner ramp.	8A
Laminated fecal pellets grainstone (M7)	Sparite matrix. Pellets (80-90%). Few miliolids.	Thin beds 10-15cm thick. Planar laminations.	Low energy restricted lagoon with low sedimentation rate.	7G, 7H
Algal bindstone (M8)	Algal laminites. Fenestrate pores, evaporite pseudomorphs and quartz.	Beds of 10-30cm thick. Dark grey and fine carbonate. Planar laminations. Exposure surfaces.	Intertidal zone. Inner ramp.	8B, 8C, 8D
Stromatolites (M9)	Domal fenestrate algal bindstone. Evaporite pseudomorphs. Fenestrate pores. Exposure couplets.	Beds of 10cm thick. Domal and wavy laminations. Exposure surfaces.	Intertidal zone. Inner ramp.	8E, 8F
Dolomudstone (M10)	10-20µm dolomite crystals (90-95%).	Highly porous beds between 10 and 20cm thick.	Intertidal zone. Inner ramp.	8G
3. Shallow lagoon with connection with open-marine facies association				
Echinoids wackestone/packstone (M11)	Mud matrix, echinoid spine and plates, oysters, bryozoas, bivalves, miliolids, ostracods and rotaliids. Quartz and chert grains.	10-20cm thick beds. With local bioturbated mud.	Low energy open lagoon. Inner ramp.	8H
Bioclastic peloidal grainstone (M12)	Sparite matrix. Peloids (70-80%) and the minor amount of bioclasts including bivalves, echinoids, miliolids, rotaliids, ostracods, bryozoans and ooids.	Thin beds between 10 and 15cm thick.	Moderate energy and normal salinity shallow lagoon connected to open marine conditions.	9A
4. Near-shore facies association				

Bivalve rudstone (M13)	Mud and sparite matrices. Bivalves, rotaliids, miliolids, ostracods, gastropods, barnacles, oysters and local red algae. Local echinoids and evaporite rosette. Micritic envelopes, micro-borings, peloidal micrite and detrital quartz grains are very common.	Very coarse-grained texture (20-50cm thick). Local planar laminations and ripple marks.	High energy and wave-agitated shoreline.	9B, 9C
Peloidal ooidal grainstone (M14)	Sparite matrix. Peloids/pellets (50%), ooids (40%) and rare bioclasts.	The rock of this microfacies is medium to coarse sand-grade 20-40cm thick. Poorly developed cross beddings. Bad sorting.	Moderate energy, edges of sand shoals and shoreface zone.	9D
Bioclastic calc-arenite (M15)	Mud and sparite matrices. Quartz, feldspar minerals, lithoclasts, miliolids, rotaliids, ostracods, barnacles, bivalves, echinoids and oyster.	Beds between 10cm and 1m thick. Laminations, cross beddings, ripple marks, flute casts and load casts. Graded beddings and bioturbations.	Marginal marine and coast environments. Inner ramp.	9E, 9F
5. Ooidal sand shoal facies association				
Oolitic grainstone (M16)	Sparite matrix. Normal and concentric ooids (80-90%). Foraminifera, quartz, chert and pellets nuclei of the ooids. Meniscus, peloidal and micritic cements and micritic envelopes.	Beds of 30-50cm thick. Coarse-grained texture Laminations, cross beddings, trough cross beddings and ripple marks. Stylolites.	High energy sand shoals and beaches. Inner ramp.	9G, 9H, 10A, 10B, 10C

Figure 1

Click here to access/download;Figure;Fig 1.tif

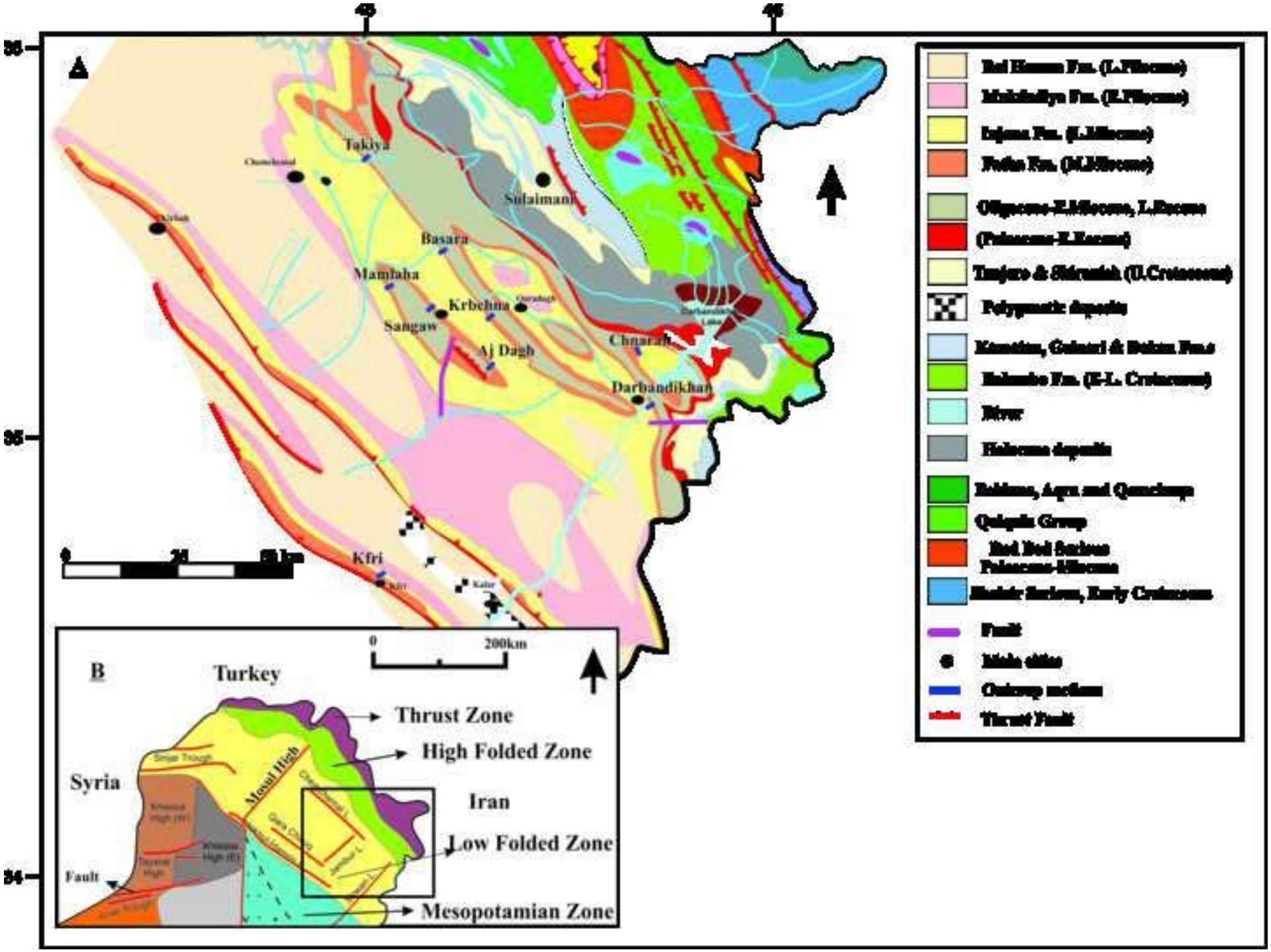

Figure 2

Click here to access/download;Figure;Fig 2.tif

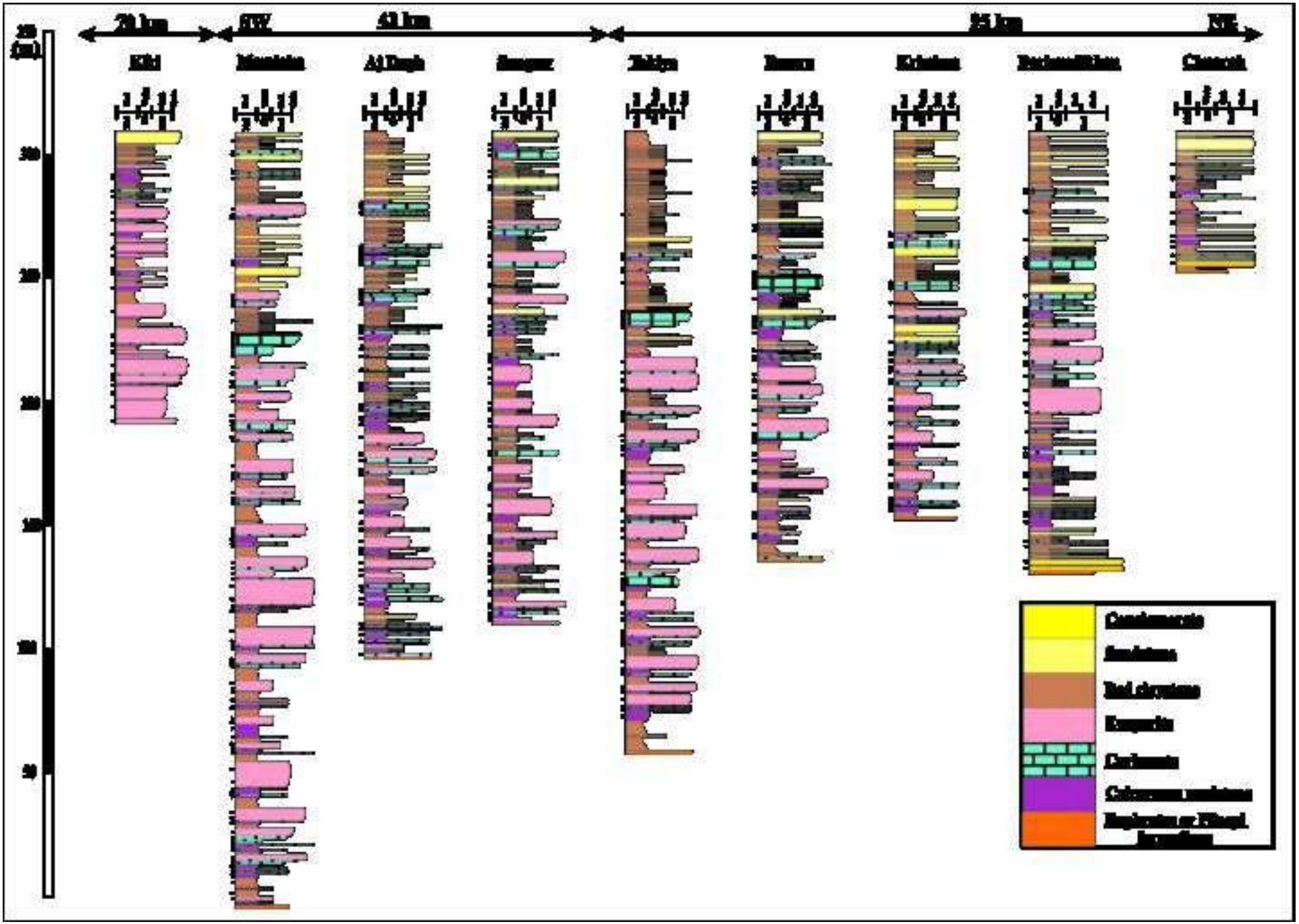

Figure 3

Click here to access/download;Figure;Fig 3.tif

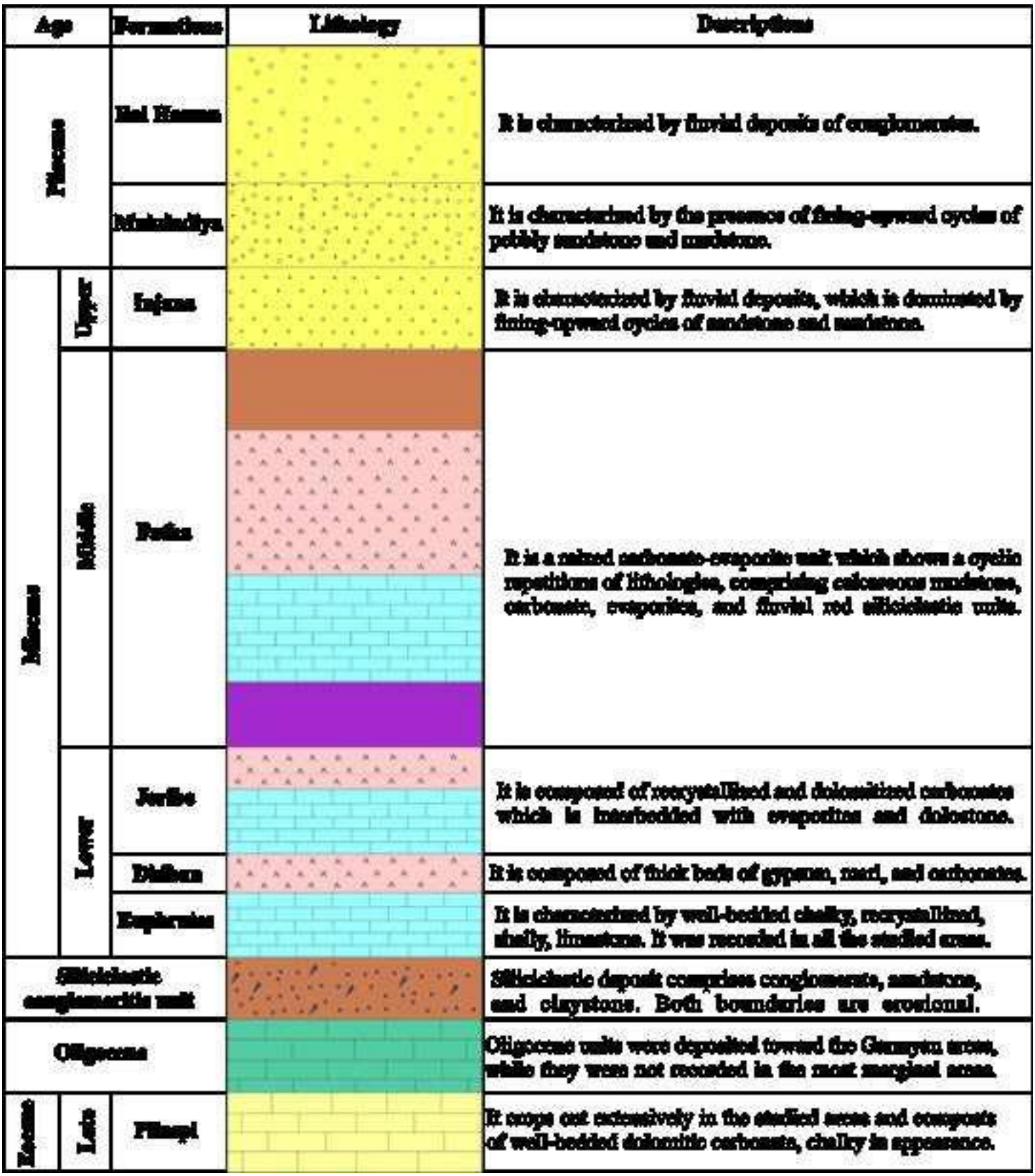

Figure 4

Click here to access/download;Figure;Fig 4.tif

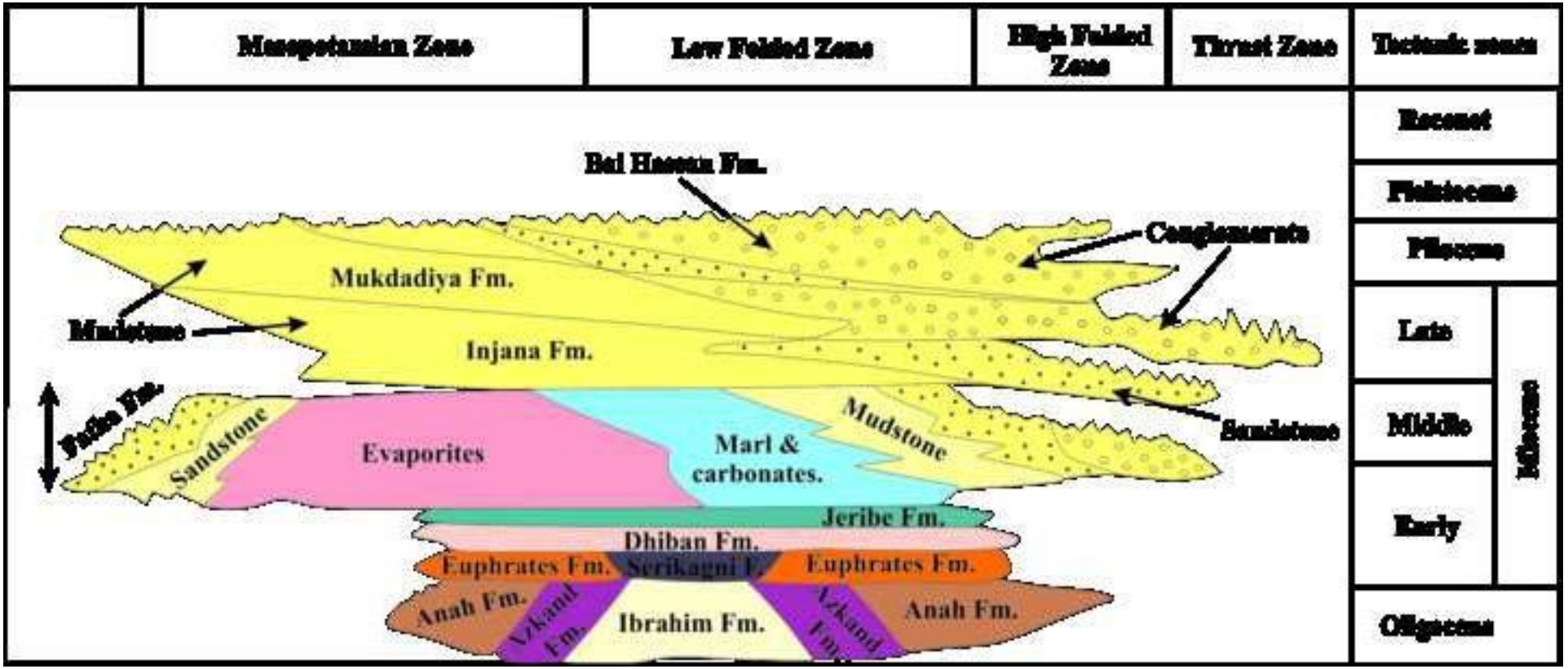

Figure 5

Click here to access/download;Figure;Fig 5.tif

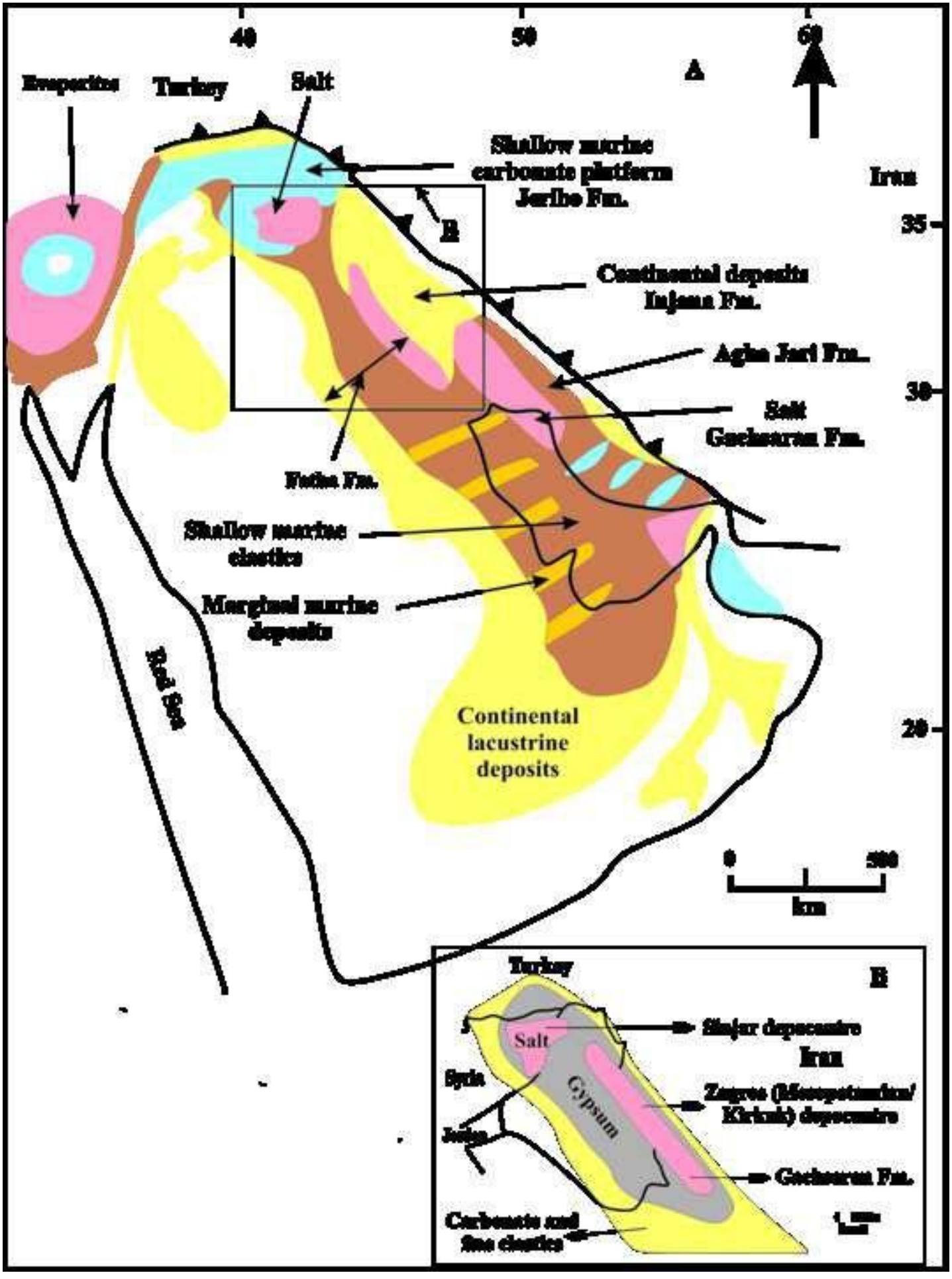

Figure 6

Click here to access/download;Figure;Fig 6.tif

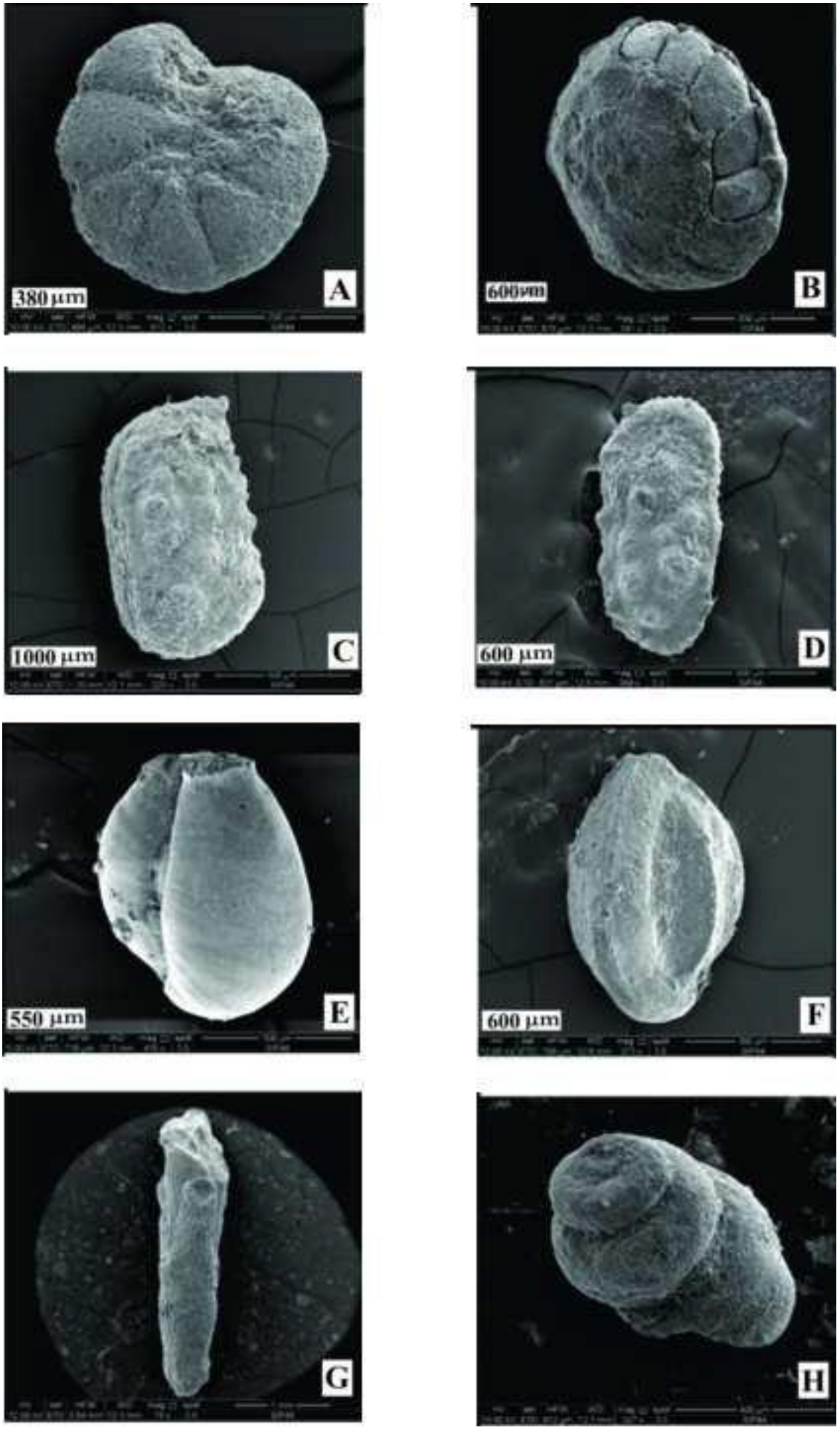

Figure 7

Click here to access/download;Figure;Fig 7.tif

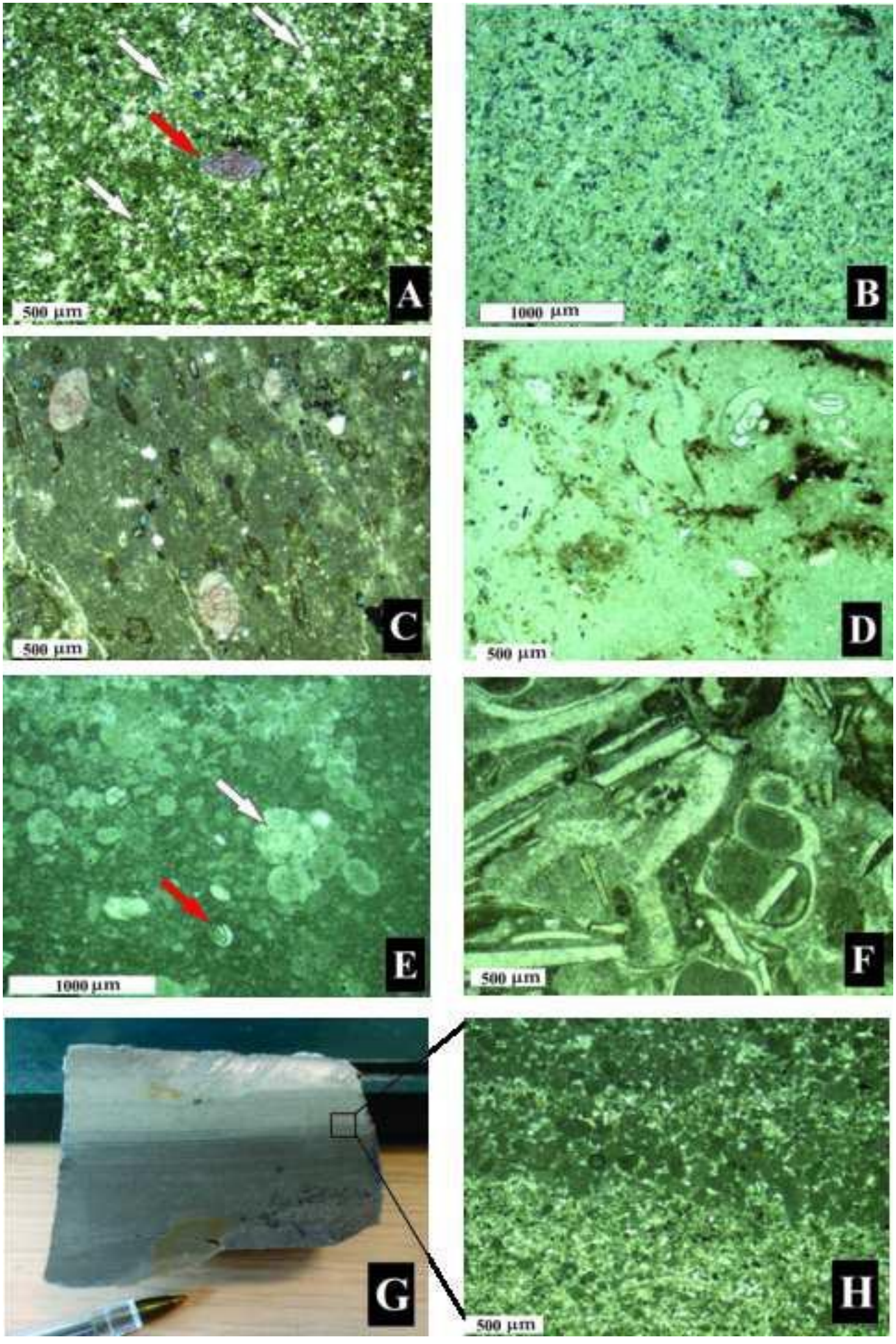

Figure 8

Click here to access/download;Figure;Fig 8.tif

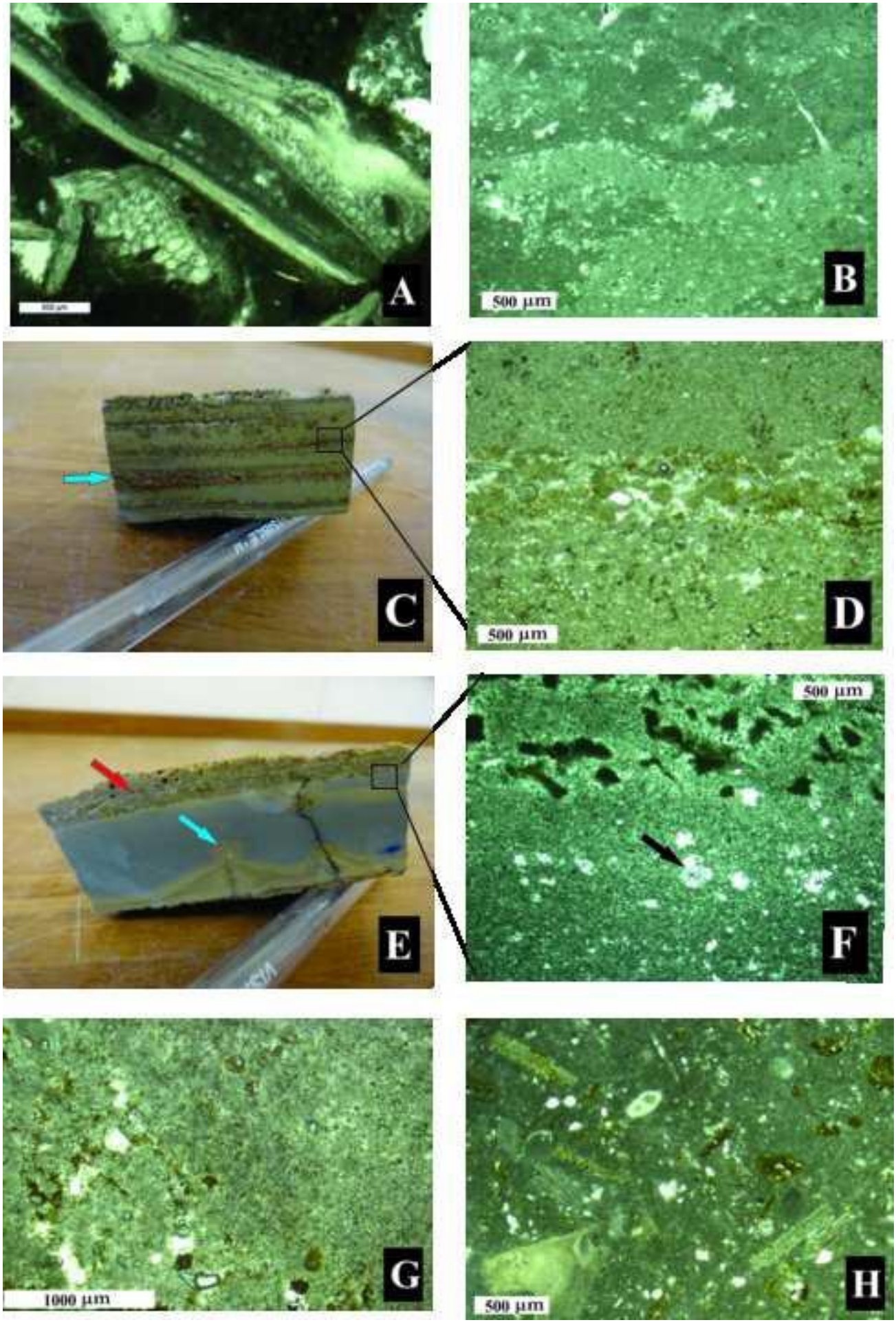

Figure 9

Click here to access/download;Figure;Fig 9.tif

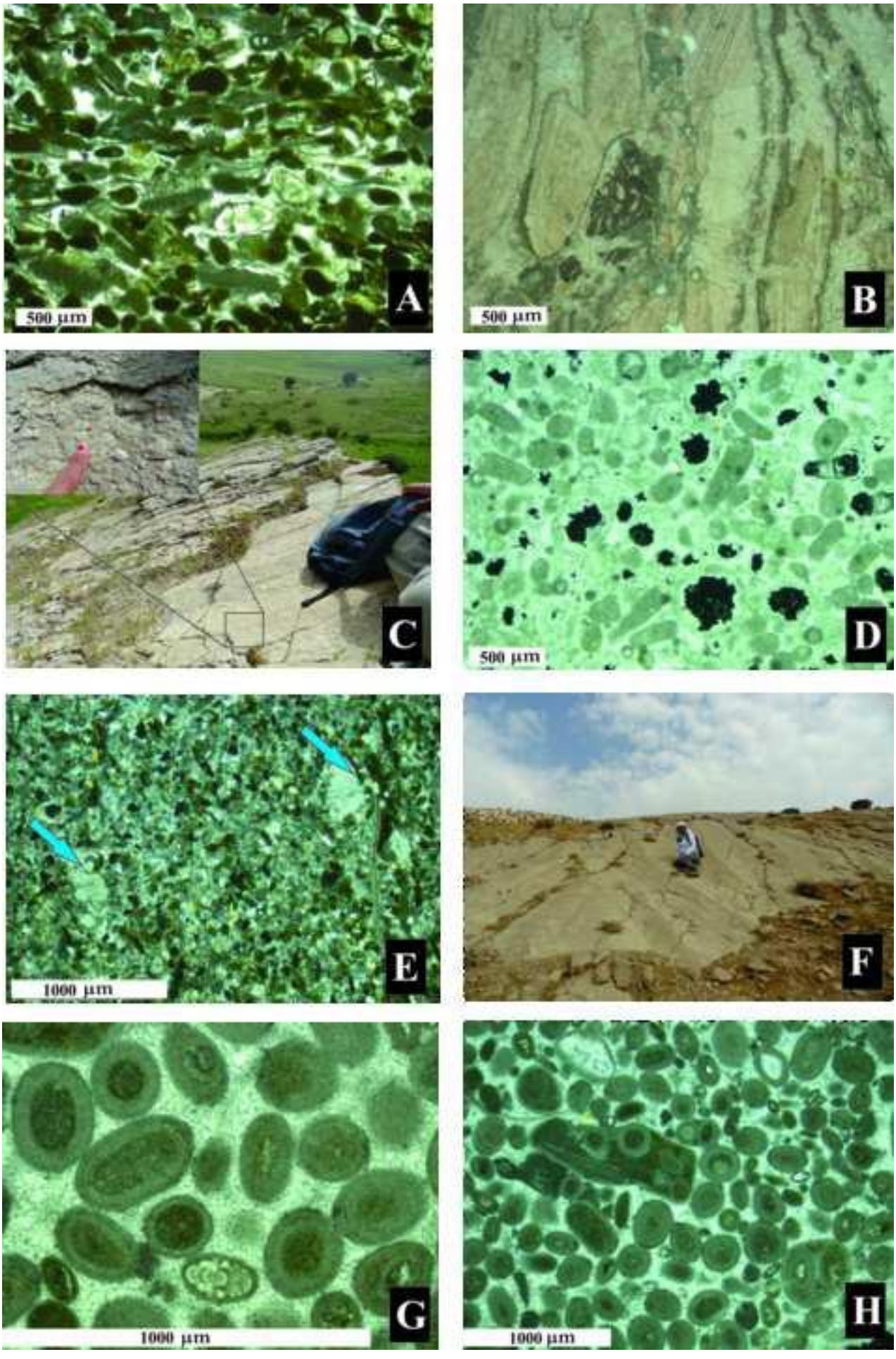

Figure 10

Click here to access/download;Figure;Fig 10.tif

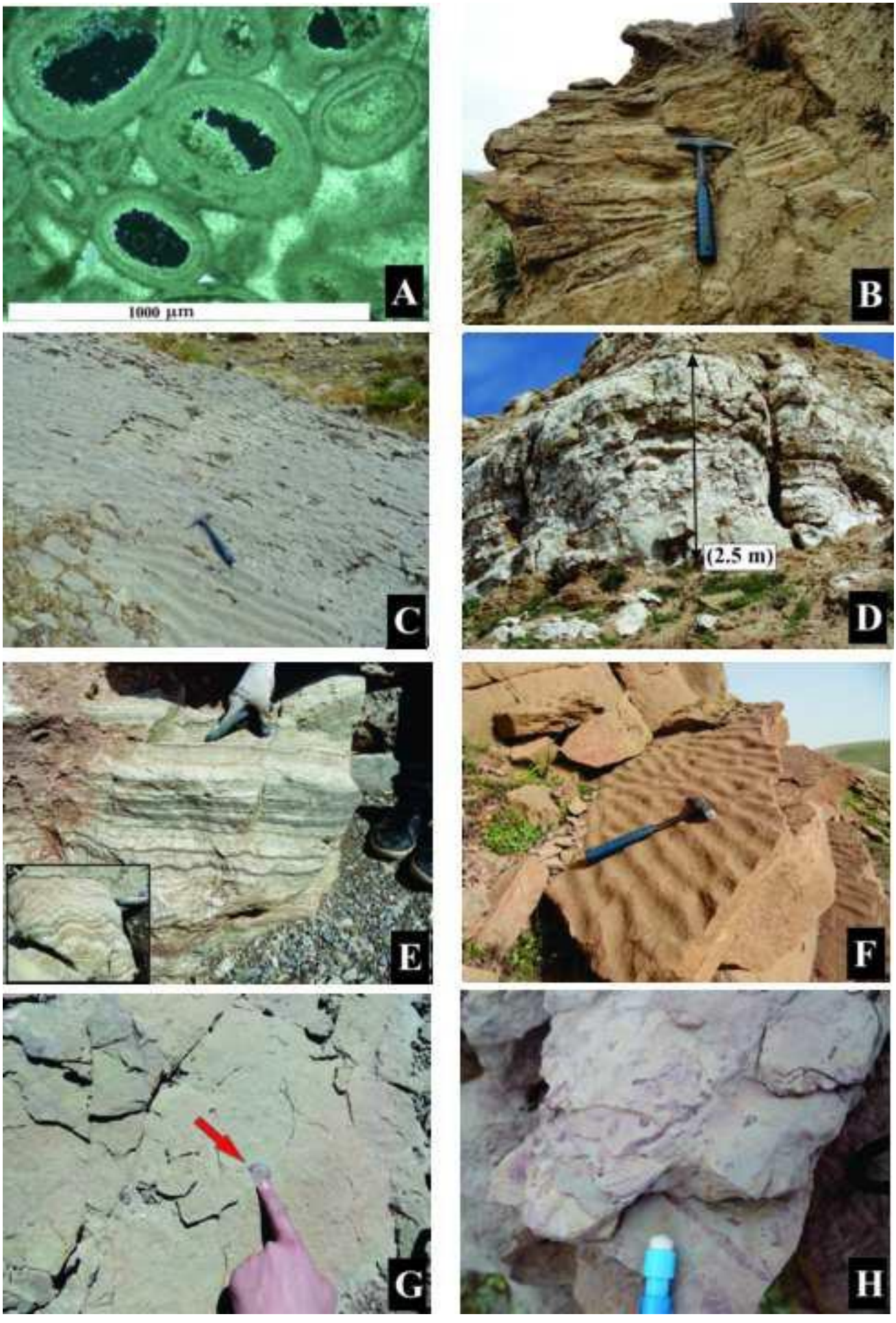

Figure 11

Click here to access/download;Figure;Fig 11.tif

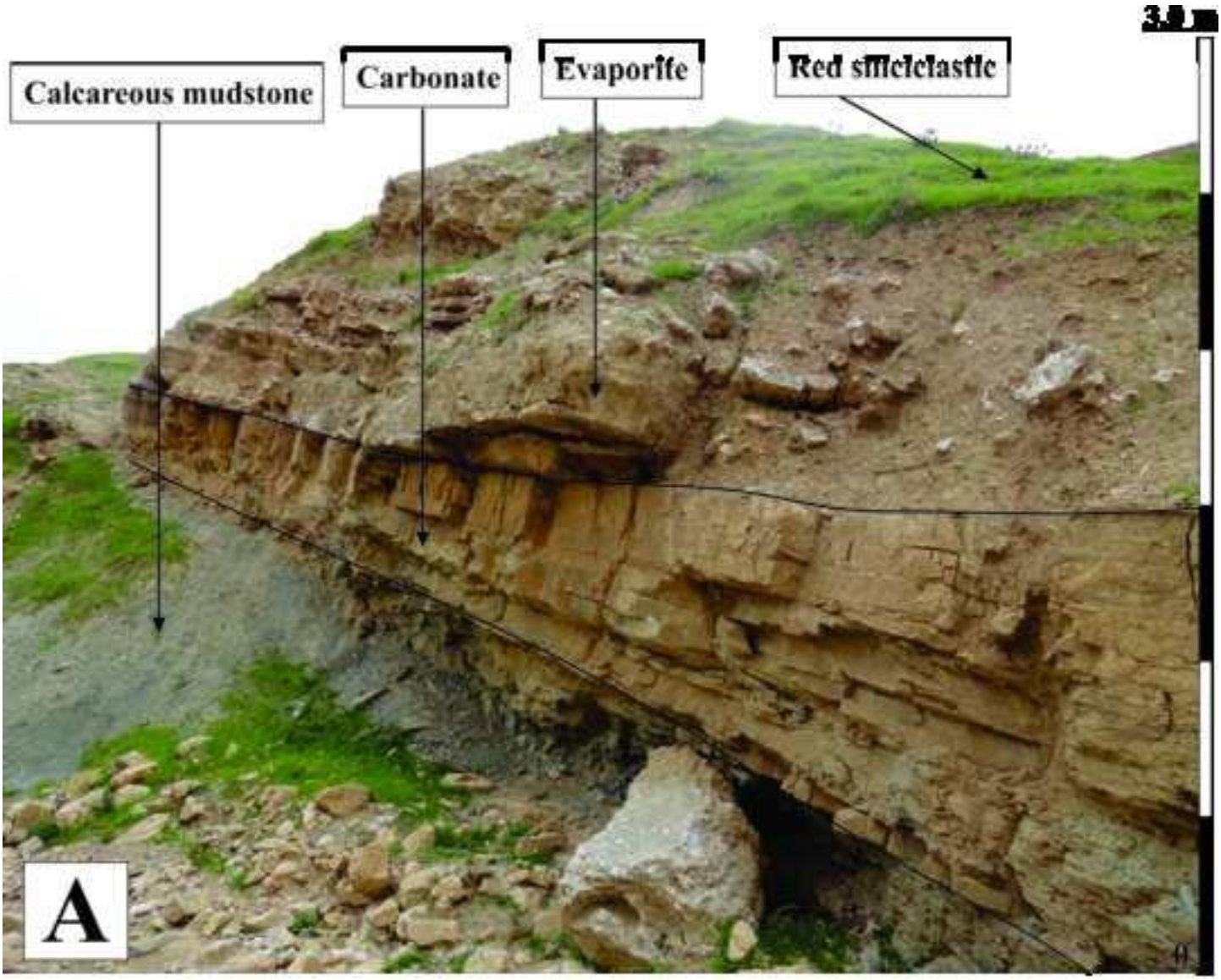

Figure 12

2

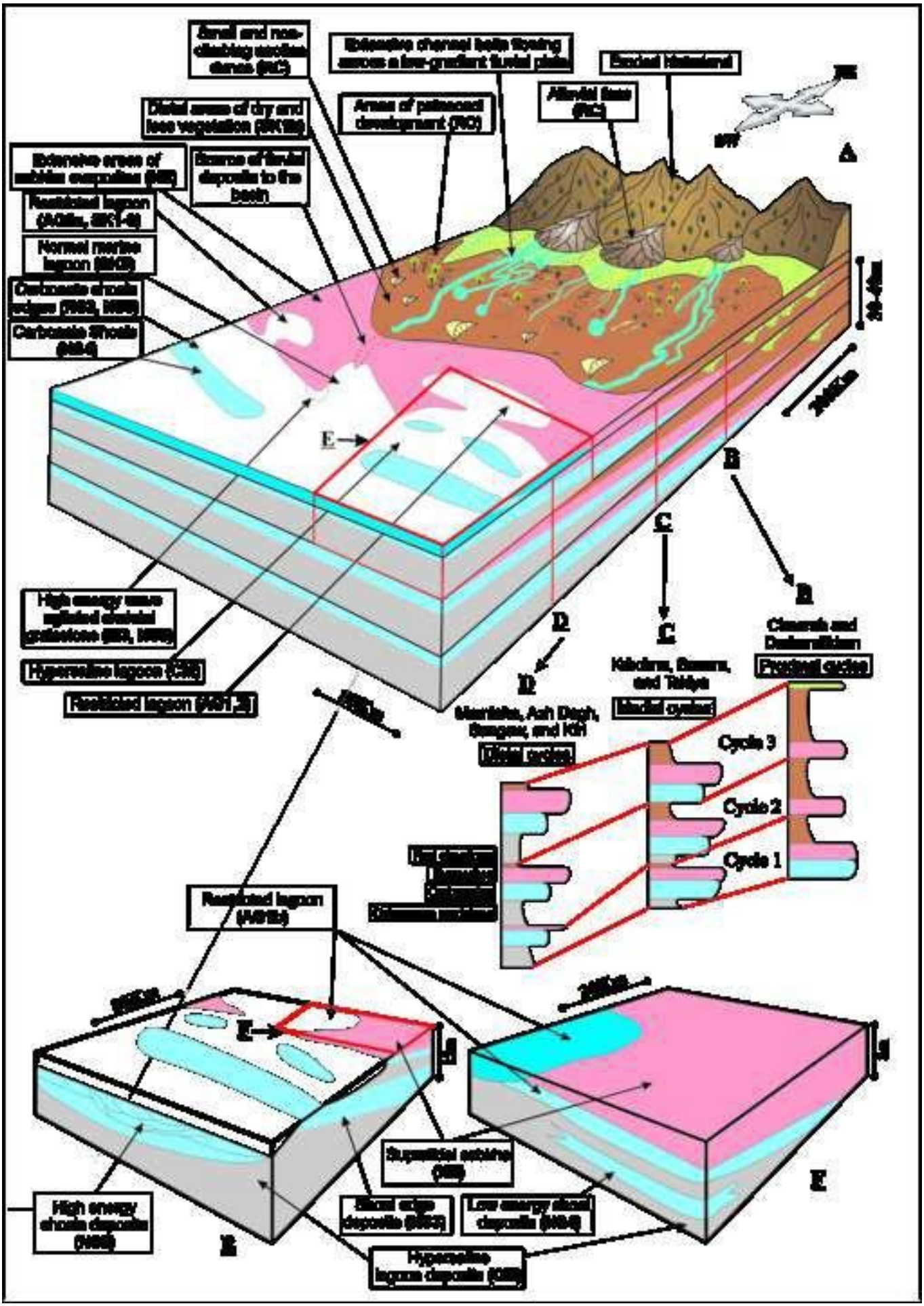

Small and non-climbing aeolian dunes (RC)
Extensive channel belts flowing across a low-gradient fluvial plain
Eroded Hatesland
Alluvial fans (RC)
Distal areas of dry and less vegetation (SK1b)
Areas of paleosol development (RO)
Extensive areas of sabkha evaporites (SE)
Source of fluvial deposits to the basin
Restricted lagoon (AG1a, SK1-3)
Normal marine lagoon (SK3)
Carbonate shoals edges (NS3, NS5)
Carbonate Shoals (NS4)
High energy wave agitated skeletal grainstone (SS, NS5)
Hypersaline lagoon (CS)
Restricted lagoon (AG1,2)
Restricted lagoon (AG1b)
Superficial sabkha (SE)
Shoal edge deposits (NS3)
Low energy shoal deposits (NS4)
High energy shoals deposits (NS5)
Hypersaline lagoon deposits (CS)
Cycle 3
Cycle 2
Cycle 1
Proximal cycles
Medial cycles
Distal cycles